doi.org/10.1002/batt.202100034

Special Collection

Zinc-Ion Hybrid Supercapacitors: Progress and Future Perspective

Xuefei Gong[+],[a] Jingwei Chen[+],[a, b] and Pooi See Lee*[a, b]

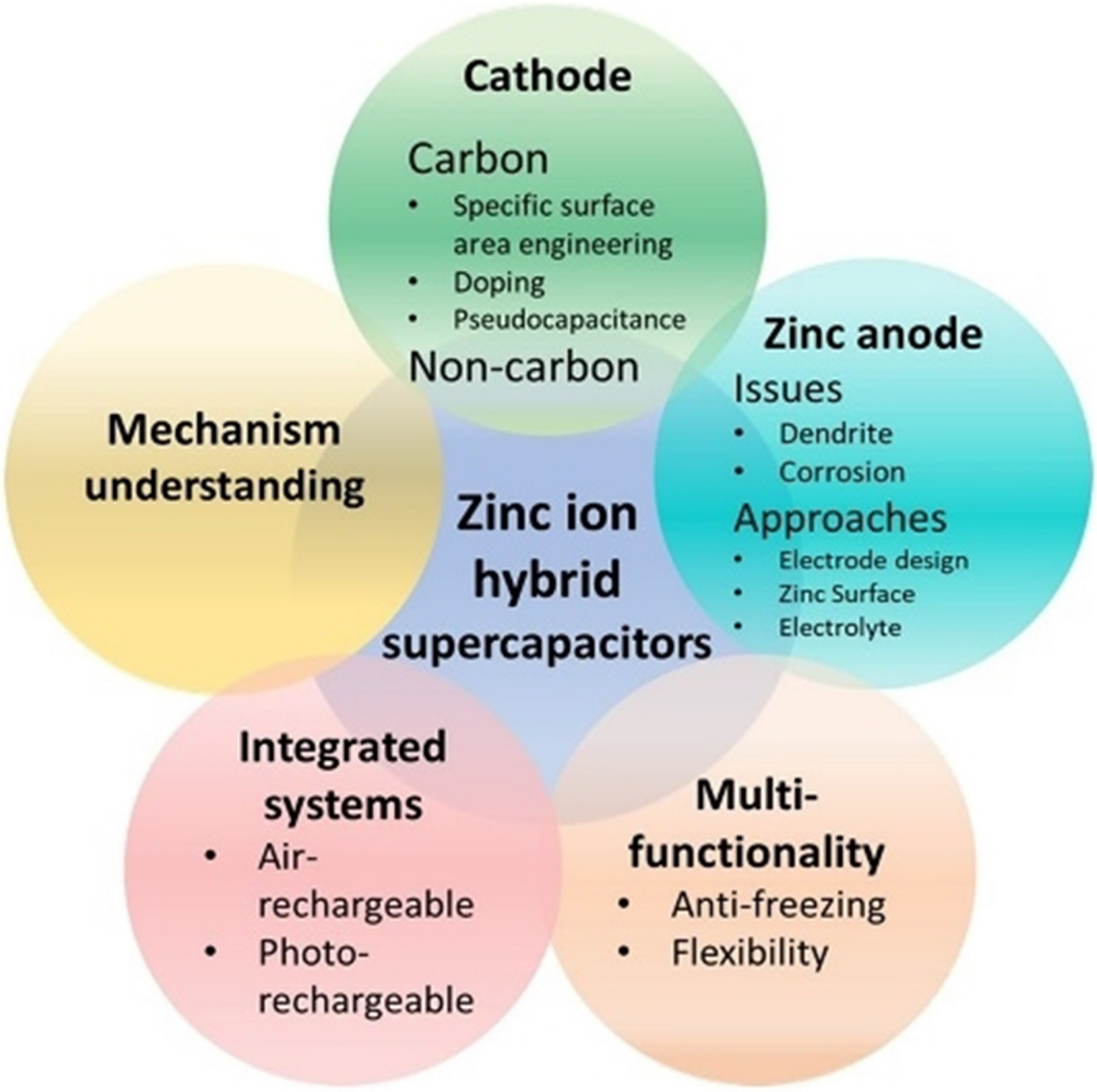

The increasing concern on the safety risks associated with the flammable organic electrolytes in alkali-ion batteries and the pursuit of both high energy density and power density in one device has spurred the investigation of aqueous multivalent metal ion hybrid supercapacitors. Zinc-ion hybrid supercapacitors (ZIHSCs) have the advantages of low standard potential, high theoretical capacity and good safety in aqueous electrolytes. In this review, the recent advancements achieved in ZIHSCs have been summarized and discussed. The progress in cathode, anode, electrolyte and the approaches adoptable to improve the electrochemical performance of ZIHSCs have been categorized. Mechanism investigation through different ex-situ and in-situ methods, incorporation of multi-functionality and integration are also demonstrated. Adoption of more in-situ characterization methods to understand the electrochemical mechanism of ZIHSCs is encouraged. Future development of ZIHSCs with higher active materials utilization rate and power output for practical applications is envisioned, assembly of ZIHSCs with more functionality is also expected.

1. Introduction

Recent decades have embraced the exploded development of energy storage devices, due to the increasing demands in portable electronics, electric vehicles, wearable electronics and miniaturized devices, etc.[1] Energy storage devices based on different configurations operate with respective merits. Among them, Li-ion batteries (LIBs) and supercapacitors (SCs) are two representatives that excel in energy density and power density, respectively.[2] However, in scenarios when both energy density and power density are required, neither LIBs nor SCs alone are qualified. This inspired the development of hybrid SCs (HSCs), which combines the merits of both batteries and SCs, marking an intriguing spot (right-top corner) in the Ragone plot.[3]

HSCs are often named after the shuttling cations, for example, lithium-ion capacitors, sodium-ion capacitors, potassium-ion capacitors, etc. HSCs are assembled with two electrodes based on different charge storage mechanisms, one is battery-type electrode (intercalation/de-intercalation, or conversion), the other one is capacitor-type electrode (non-Faradaic adsorption/desorption or Faradaic redox reaction near the surface).[4] There has been extensive evaluation of different monovalent HSCs, usually based on organic solvents that offer wide electrochemical window.[5] However, organic solvents often suffer from flammability and limited ionic conductivity, while the capacity and kinetics mismatch between cathode and anode will also affect the overall performance of monovalent HSCs.[2c,6] In addition, the limited abundance and non-uniform distribution of Li source on earth crust has triggered increasing concern of the supply risks of Li.[6] As alternatives, multivalent HSCs based on Zn^{2+}, Mg^{2+} and Ca^{2+} are drawing more and more attention.[7] These multivalent HSCs allow the use of less reactive metals as anodes and incorporation of aqueous electrolyte with high ionic conductivity, mitigating latent safety issues and increasing the power output.[8] Among multivalent HSCs, zinc ion hybrid supercapacitors (ZIHSCs) are one of the most promising candidates, due to the low standard potential (−0.76 V vs standard hydrogen electrode), high theoretical capacity (820 mAh/g; 5845 Ah/L), low cost and environmentally friendliness..[7a,8–9] Other candidates such as Mg has a low standard potential of −2.37 V, with high theoretical gravimetric/volumetric capacity (2205 mAh/g; 3833 Ah/L). However, the choice of electrolyte for reversible Mg plating/stripping is limited, and the increased electrostatic effect of divalent Mg^{2+} will lead to slow solid-state kinetics, affecting the capacity and power output. Similarly, calcium with low standard potential of −2.87 V also has high theoretical gravimetric/volumetric capacity (1337 mAh/g; 2073 Ah/L). Nonetheless, plating of Ca is hindered due to the easily formed passivation layer in organic electrolytes. The low standard potential of Mg/Mg^{2+} and Ca/Ca^{2+} also limited the use of pure metal as anodes in aqueous electrolytes. For the trivalent Al-based HSCs, the standard potential is higher (−1.67 V), and the theoretical gravimetric/volumetric capacity (2980 mAh/g; 8046 Ah/L) are the highest amongst multivalent HSCs. Al is also one of the most abundant metal on Earth's crust. Aqueous electrolytes can be employed for Al^{3+} based energy storage, however, the easily formed passive oxidation layer on Al will hinder the plating of Al^{3+} and there is often accompanied hydrogen evolution at the anode. The most widely used electrolytes for Al^{3+} energy storage are $AlCl_3$ dissolved in ionic liquids.

Given the above-mentioned merits of ZIHSCs, the development of ZIHSCs is still in its infancy stage. Construction of ZIHSCs still relies heavily on exploitation of electrode materials that offer high capacity and good electrochemical stability, electrolyte that allows fast kinetics and reversible Zn^{2+} stripping/plating, and Zn anode structures that avoid the formation of dendrites. In the meantime, there are often zinc salt byproducts formed on electrode materials during extended cycling that causes degradation of ZIHSCs, and the in-depth mechanism understanding of ZIHSCs is still lacking. In this review, as schemed in Figure 1, recent progress achieved in

[a] Dr. X. Gong,[+] Dr. J. Chen,[+] Prof. P. S. Lee
School of Materials Science and Engineering
Nanyang Technological University
Singapore 639798, Singapore
E-mail: pslee@ntu.edu.sg
[b] Dr. J. Chen,[+] Prof. P. S. Lee
Singapore-HUJ Alliance for Research and Enterprise (SHARE)
Nanomaterials for Energy and Energy Water Nexus (NEW)
Campus for Research Excellence and Technological Enterprise (CREATE)
Singapore 138602, Singapore
[+] These authors contributed equally to this work.

Special Collection An invited contribution to a Special Collection dedicated to Metal-Ion Hybrid Supercapacitors

doi.org/10.1002/batt.202100034

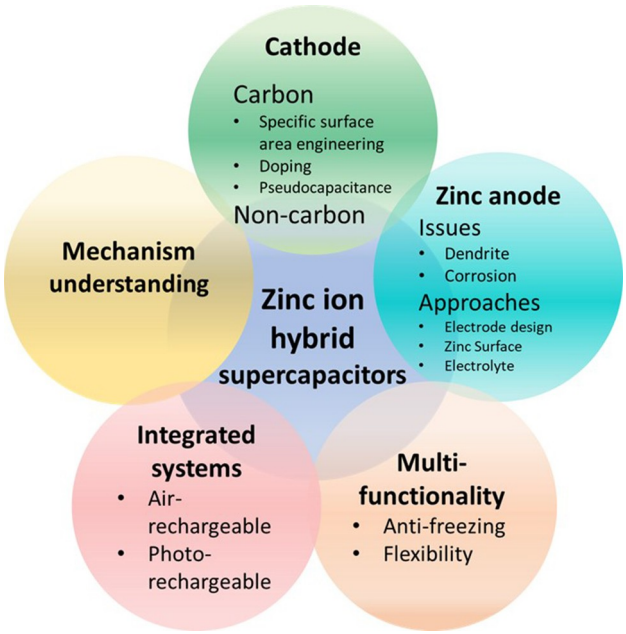

Figure 1. Summary of the aspects discussed in this review.

developing novel electrode materials (cathode including carbon and non-carbon materials, zinc anode) and the approaches to improve the performance of ZIHSCs will be summarized. Mechanism understanding of ZIHSCs through different ex-situ and in-situ techniques will be discussed. Realization of multifunctional ZIHSCs (anti-freezing, flexible) and integrated systems will also be showcased. More focus should be paid to realize better mechanism understanding of ZIHSCs by employing in-situ characterization techniques, and to construct ZIHSCs that are deformable, self-healable and biodegradable, etc.

2. ZIHSC Cathode

2.1. Carbon Materials

ZIHSCs are mostly based on battery-type Zn metal as the anode with physical adsorption-based carbon materials as the cathode. Carbon materials with high surface area, good electrochemical stability, low cost and high electronic conductivity are deemed as promising cathode materials for ZIHSCs. However, commercial activated carbon, e.g. YP-50F and AC (Kurraray, Japan) do not necessarily offer competitive electrochemical performance in Zn-ion containing electrolyte. For example, YP-50F delivered 55 mAh/g (at 0.5 A/g) and 17.2 mAh/g (at 20 A/g) in 1 M $ZnSO_4$ aqueous electrolyte.[10] Different approaches have been adopted to improve the charge storage capability of carbon cathodes for ZIHSCs, including surface area and pore structure engineering, heteroatom doping, and pseudocapacitance incorporation, which will be discussed in detail in the following sections.

2.1.1. Surface Area and Pore Structure Engineering

The synthesis of carbon materials often involves high temperature pyrolysis of precursors and subsequent activation. As ZIHSC cathode based on physical ion adsorption/desorption mechanism, carbon materials with higher specific surface area (SSA) and abundant micropores/mesopores are preferable towards better charge storage capability. To achieve this goal, the synthesis condition of the carbon materials has been fine-tuned, through optimizing activation content/species, employing new precursors, and adjusting pyrolysis temperature, etc.

Activated carbon (AC) derived from coconut-shell carbonization was subsequently activated with different amount of KOH. Higher amount of KOH can effectively increase the SSA from 2596 to 3354 m^2/g, thus allowing improved charge storage performance from 130 F/g to 153 F/g.[7b] The content of

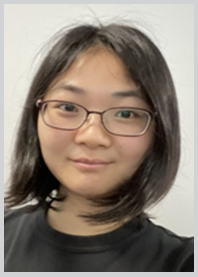

Xuefei Gong received her Ph.D. degree under the supervision of Prof. Pooi See Lee at the School of Materials Science and Engineering, Nanyang Technological University, Singapore. She is currently a research fellow at Nanyang Technological University. Her research focuses on flexible energy storage devices for wearable applications.

Jingwei Chen obtained his Ph.D. from the School of Materials Science and Engineering in Nanyang Technological University in 2019, under the supervision of Prof. Lee Pooi See. He is currently a research fellow in Prof. Lee Pooi See's research group. His research focuses on designing novel electrode materials for electrochemical energy storage and conversion devices, including metal-ion batteries and electrochromic devices.

Pooi See Lee received her Ph.D. from National University of Singapore in 2002. She joined the School of Materials Science and Engineering, Nanyang Technological University as an Assistant Professor in 2004. She was promoted to tenured Associate Professor in 2009 and full Professor in 2015. Her research focuses on nanomaterials for energy and electronics applications, flexible and stretchable devices, electrochemical inspired devices, and human-machine interface.

KOH was also increased to activate the carbonized waste polyurethane foam, producing mesoporous carbon (MPC) with higher SSA and more mesopores.[11] MPC with the highest SSA can realize capacity of 209 F/g at 0.2 A/g as ZIHSC cathode.[11] KOH as activation agent is highly corrosive and progressive in pore opening, yet there is difficulty in controlling the morphology of the final products.[11–12] Other mild activation agents were also adopted to obtain porous carbon. A KNO_3 assisted-KOH activation approach was employed to synthesize porous carbon nanosheets (PCNs) from starch powders.[12b] Incorporation of KNO_3 can allow the formation of nanosheets with increased SSA and more micropores and mesopores. In PCNs with suitable micropores content, optimum charge storage can be obtained, demonstrating capacity of 149 mAh/g at 0.2 A/g and 75 mAh/g at 20 A/g.[12b] Porous carbon nanoflakes (PCNFs) were prepared through carbonization and activation of the sodium polyacrylate and mild $KHCO_3$ mixture. Higher amount of $KHCO_3$ can introduce more defects and higher surface area, higher porosity as well as higher O content in PCNFs.[12a] With suitable amount of $KHCO_3$, the nanocage morphology was transformed into nanoflakes with well-balanced micropores and mesopores content, rendering capacity of 177.7 mAh/g at 0.5 A/g with 85.5 mAh/g maintained at 20 A/g.[12a]

Aside from adjusting the amount/species of activating agents, different precursors were also employed to produce carbon materials. As shown in Figure 2(a), Zaipen et al. employed a soft-template (TX-100) to construct hollow carbon spheres (HCSs) by pyrolysis of PACP (polyaniline-*co*-polypyrrole) co-polymer hollow sphere precursor. Solid carbon nanoparticles (SCNs) were also prepared without the soft template.[13]

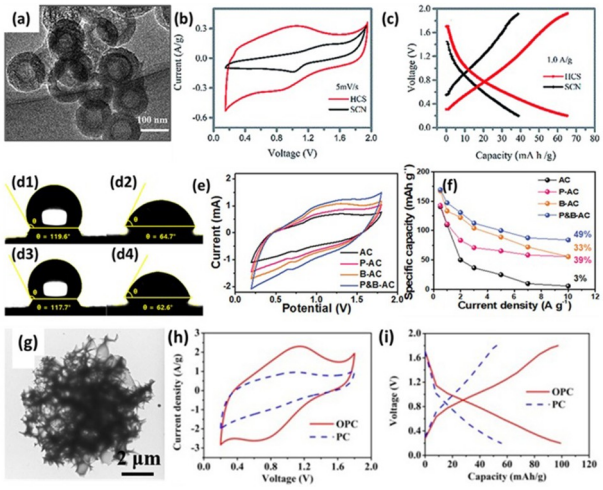

Figure 2. Carbon materials for ZIHSC cathode. a) Transmission electron microscopy (TEM) image of hollow carbon spheres (HCSs). b–c) Cyclic voltammogram (CV) and galvanostatic charge-discharge (GCD) curves of HSC and solid carbon nanoparticles (SCNs). Reproduced from Ref. [13] with permission. Copyright 2019, Royal Society of Chemistry. Contact angle of d1) bare activated carbon (AC), d2) P-doped AC, d3) B-doped AC, d4) P, B co-doped AC. e) CV curves and f) specific capacity at different current densities of AC, P-AC, B-AC, P&B-AC. Reproduced from Ref. [14] with permission. Copyright 2020, American Chemical Society. g) TEM image of oxygen-enriched porous carbon (OPC). h–i) CV and GCD curves of OPC vs PC. Reproduced from Ref. [15] with permission. Copyright 2020, Elsevier.

The as-obtained HSCs have larger number of defects and higher SSA (819.5 m^2/g) than SCNs (246.7 m^2/g). As a result, HSCs deliver larger integrated area in the CV curves and longer charge/discharge time in the GCD profiles as shown in Figure 2(b–c). At the same current density of 1 A/g, HCSs can realize capacity of 65.1 mAh/g while SCNs only deliver 38.8 mAh/g.[13] Two kinds of bio-precursors (coconut shell and bagasse) were mixed for subsequent carbonization and activation to produce hierarchical porous carbon (HPC).[16] The mixed precursors allow formation of HPC with higher SSA, larger pore volume, abundance of mesopores and better electronic conductivity than those of porous carbons derived from single precursor (PC–B from bagasse; PC-CS from coconut shell). As a result, HPC delivered obviously improved electrochemical performance in 2 M $ZnSO_4$ (+1 M Na_2SO_4) aqueous electrolyte, with capacity of 204 mAh/g at 0.2 A/g and 101 mAh/g at 5 A/g, in comparison to the inferior performance of PC–B (179 mAh/g at 0.2 A/g; 45 mAh/g at 5 A/g) and PC–CS (125 mAh/g at 0.2 A/g; 59 mAh/g at 5 A/g).[16] Different amount of polyvinylpyrrolidone (PVP) was coated onto AC, producing mesoporous structured AC (MSAC) through dehydrogenation process. Suitable amount of PVP-coating can create high SSA and more mesopores for shorter ion diffusion pathway, as well as higher O content with lowered electrolyte contact angle.[17] The optimum MSAC demonstrated better charge storage capability as ZIHSC cathode in 2 M $ZnSO_4$ aqueous electrolyte, with specific capacity of 176 mAh/g at 0.5 A/g and 72.3 mAh/g at 10 A/g.[17]

Activation/carbonization temperature will also affect the microstructures of the final carbon materials. For example, activating pencil-shavings derived carbon (PSC) at appropriate temperature can result in higher surface area, more defects and higher O-content.[18] The optimized activated PSC (PSC-A600, activated at 600 °C) demonstrated capacity of 183.7 mAh/g at 0.2 A/g and 81.8 mAh/g at 20 A/g in 1 M $Zn(CF_3SO_3)_2$ aqueous electrolyte, superior to those of PSC-A700 (146.6 mAh/g at 0.2 A/g and 43.5 mAh/g at 20 A/g) and PSC-A500 (155.3 mAh/g at 0.2 A/g and 36.6 mAh/g at 20 A/g).[18] Similarly, pyrolysis of pyromellitic acid tetra-potassium salt (PMA4K) at higher temperature can lead to formation of PC with higher SSA and porosity but lower O-content.[19] PC700 (pyrolyzed at 700 °C) exhibited highest capacity of 191.5 mAh/g at 0.1 A/g in 3 M $Zn(ClO_4)_2$ aqueous electrolyte, while PC800 showed better rate performance, with capacity of 78.4 mAh/g at 20 A/g.[19]

2.1.2. Heteroatom Doping

Foreign atoms doping can introduce more active sites, mitigate agglomeration through electrostatic repulsion, allow electrolyte penetration and increase electronic conductivity in carbon cathodes.[10,20] Doping of different atoms have been achieved with different precursors/templates. N-doped hierarchical porous carbon (HPC) was obtained by activation and carbonization of chitosan precursor. N-doping offers large number of active sites and facilitates electrolyte infiltration, enabling much higher capacity (136.8 mAh/g at 0.1 A/g) and rate performance

(66.5 mAh/g at 10 A/g) in N-HPC than in commercial AC (~120 mAh/g at 0.1 A/g and ~52 mAh/g at 10 A/g) in 2 M $ZnSO_4$ aqueous electrolyte.[21] Similarly, Wu et al. employed Zn, Co bimetallic organic frameworks as precursor to synthesize N-enriched porous carbon with high N content (8.9 at.%), dominated by pyridinic N (54%). It was disclosed that compared to other N species (pyrrolic and graphitic), the pyridinic N possess larger binding energy to coordinate with Zn^{2+}, enabling better Zn-ion storage capability than N-PC with less pyridinic N.[22]

Bare AC suffers from limited electrical conductivity and wettability. An, et al. successfully introduced B, P co-doping into activated carbon with H_3BO_3 and red phosphorous as the B and P source, respectively, followed by calcination.[14] B-doping can improve the electronic conductivity of AC due the transition in electronic structure, while P-doping can improve the surface wettability with electrolyte due to increased amount of O-containing functional groups.[14] As shown in Figure 2(d), the contact angle of P-AC and P&B-AC (phosphorous and boron co-doped AC) with electrolyte is apparently smaller than those of bare AC and P-AC. As a result, as displayed in Figure 2(e–f), with larger integrated area in CV scans, P&B AC can realize obviously improved capacity (169.4 mAh/g at 0.5 A/g) and rate performance (84 mAh/g at 10 A/g) than those of the B-AC, P-AC or the bare AC in 2 M $ZnSO_4$ aqueous electrolyte.[14] With acrylonitrile copolymer as carbon source, H_3BO_3 was also employed as intercalator and template to produce two-dimensional layered B, N co-doped porous carbon (LDC).[10] With B, N co-doping, the LDC manifested optimum charge storage capability (127.7 mAh/g at 0.5 A/g; 42.8 mAh/g at 20 A/g) in 1 M $ZnSO_4$ aqueous electrolyte, superior than that of non-doped carbon (20 mAh/g at 0.5 A/g; 2.3 mAh/g at 5 A/g), rGO (27.7 mAh/g at 0.5 A/g; 6.5 mAh/g at 10 A/g) and commercial YP-50F (55 mAh/g at 0.5 A/g; 17.2 mAh/g at 20 A/g).[10]

2.1.3. Pseudocapacitance Incorporation

The charge storage mechanism of high SSA carbon materials are mostly based on physical ion adsorption/desorption, with limited capacity and energy density. Incorporation of pseudocapacitance into carbon materials through functional groups grafting helps to further improve the charge storage capability and thus the capacity and energy density of ZIHSCs.

CNT was oxidized into oCNTs (oxidized CNTs) through sequential treatment by concentrated sulfuric acid, $KMnO_4$ and H_2O_2, creating surface amorphous layer with inner graphitic structure maintained.[23] The oxygen-containing functional groups (carboxylic and hydroxyl) on the surface can adsorb/desorb Zn^{2+} during discharge/charge, respectively. As a result, oCNTs display quasi-triangle GCD (galvanostatic charge/discharge) curve and extended charging/discharging time in comparison with bare CNTs, manifesting higher charge storage capability involving Faradaic pseudocapacitance.[23] Oxygen plasma treatment of CNTs was also evidenced to increase the hydrophilicity with lower contact angle and reduce the charge transfer resistance, thus larger integrated area in CV and longer discharging time in GCD curves.[24] The introduced oxygen functional groups contribute extra pseudocapacitance through Zn^{2+} adsorption/desorption.[24]

Oxygen-enriched three-dimensional porous carbon (OPC) was obtained through acid treatment (in concentrated HNO_3) of PC as shown in Figure 2(g), increasing the O content from 11.87% to 19.87% through introduction of multiple oxygen-containing functional groups (e.g. quinone, phenol, ether, ester, etc.).[25] As can be evidenced from the large area in CV scans and longer charge/discharge time of OPC than PC in Figure 2(h-i), higher O content endows better charge storage capability of OPC (99.1 mAh/g at 0.5 A/g) than PC (55.7 mAh/g at 0.5 A/g) in 1 M $ZnSO_4$ aqueous electrolyte (with 1 wt.% gelatin), due to the dominating Faradaic contribution by surface O-containing functional groups.[25] Different activation temperature was also found to alter the O content in pencil shavings derived porous carbon (PSC). The presence of the oxygen-containing functional groups can increase the hydrophilicity and introduce extra pseudocapacitance. The oxygen content in non-activated PSC was improved from 10.8% to 14.7% in the PSC activated at 600 °C with higher surface area and abundance of micropores, explaining the higher capacity and better rate performance in PSC-600 (183.7 mAh/g at 0.2 A/g, 81.8 mAh/g at 20 A/g, in 1 M $Zn(CF_3SO_3)_2$ aqueous electrolyte) than PSC (~12.9 mAh/g at 0.2 A/g, ~1.91 mAh/g at 20 A/g).[18]

Direct pyrolysis of pyromellitic acid tetra-potassium salt followed by acid etching can also result in formation of porous carbon (PC). PC800 (pyrolyzed at 800 °C) demonstrates typical physical ion adsorption/desorption charge storage behavior in voltage range of 0.5–1.5 V in 3 M $Zn(ClO_4)_2$ aqueous electrolyte, with capacitance of 99.5 F/g (at 20 mV/s). By expanding the voltage window to 0–1.9 V, both reversible hydrogen adsorption/desorption (~0–0.2 V) and reversible oxidation/reduction of surface carbon atoms or oxygen functional groups (~1.7–1.9 V) were incorporated, increasing the capacitance to 133 F/g under the same scan rate.[19] The incorporation of these two redox reactions were verified through different means of analysis, which will be discussed later in Section 3.

2.2. Non-Carbon Materials

The above-discussed ZIHSCs are mostly constructed with adsorption/desorption-based carbon-cathode and battery-type Zn metal anode. Aside from carbon, other non-carbon materials including inorganic MXene, metal oxides, phosphorene, and organic polymers etc. have also been attempted as cathode to construct ZIHSCs.

2.2.1. MXenes

MXene with two-dimensional morphology and good electrical conductivity and hydrophilicity is an intriguing cathode for ZIHSCs. Zhi et al. employed Ti_3C_2 freestanding paper as the

cathode for ZIHSCs, the anode of which is obtained by electrodeposition of Zn nanosheets on Ti_3C_2 paper. This Ti_3C_2 paper based ZIHSCs delivered specific capacity of 132 F/g at 0.5 A/g and 118 F/g at 3 A/g in 1 M $ZnSO_4$ aqueous electrolyte (with 1 wt.% gelatin).[32] In order to mitigate the aggregation/stacking issue, MXene-rGO composite aerogel was obtained through soaking rGO aerogel in $Ti_3C_2T_x$ MXene dispersion and subsequent freeze-drying.[33] The weight content of MXene in the composite aerogel was optimized to be 26% (Mxene-rGO_2), with the smallest charge transfer resistance and fast kinetics. High content of MXene can increase electrical conductivity and hydrophilicity, at the sacrifice of porosity. The ZIHSCs based on Mxene-rGO_2 aerogel cathode and Zn anode manifested high specific capacitance of 128.6 F/g (0.4 A/g) in 2 M $ZnSO_4$ aqueous electrolyte, good rate performance (40.3 F/g at 6 A/g), and excellent cycling stability (95% retention after 75000 cycles).[33] V-based V_2CT_x MXene was also employed as cathode to couple with Zn for ZIHSCs, without obvious plateau observed in the GCD curves.[9] Unlike other cathode materials that suffer from capacity decay during cycling, this V_2CT_x-based cathode experienced abnormal capacity enhancement along with cycling in 21 M LiTFSI + 1 M $Zn(CF_3SO_3)_2$ aqueous electrolyte. This capacity enhancement was attributed to cycling induced delamination of the V_2CT_x that created more active sites and formation of phase transition products.

2.2.2. Metal Oxides

Commercially available amorphous $RuO_2{\cdot}H_2O$ powders were employed as cathode materials for ZIHSCs with Zn as the anode.[8a] Anhydrous RuO_2 powders were also obtained through heat treatment. As shown in Figure 3(b), $RuO_2{\cdot}H_2O$ demonstrated obvious larger integrated CV area than the anhydrous RuO_2, indicating better charge storage capability. Based on the GCD curves of $RuO_2{\cdot}H_2O$ shown in Figure 3(c), capacity of 122 mAh/g can be achieved at 0.1 A/g with 98 mAh/g retained at 20 A/g in 2 M $Zn(CF_3SO_3)_2$ aqueous electrolyte, showing excellent rate performance. The charge storage of $RuO_2{\cdot}H_2O$ is mostly based on reversible Zn^{2+} insertion/extraction with small contribution from the protons in the electrolyte. With high fraction of capacitive contribution (96.4% at 20 mV/s), both high energy density of 119 Wh/kg (at power density of ~0.1 kW/kg) and high-power density of 16.74 kW/kg (with energy density of 82 Wh/kg) can be delivered. In comparison, ZIHSCs based on the anhydrous RuO_2 can only reach capacity of 38 mAh/g at 0.1 A/g and 15 mAh/g at 20 A/g, emphasizing the importance of the structural water that facilitated ion transport.[8a]

The electrochemical mechanism of MnO_2 with Zn anode is based on the reversible Zn ion intercalation/deintercalation, with reversible redox peaks in CV scans and plateaus in GCD curves.[2c,7a] Thus, to construct ZIHSCs with MnO_2 cathode, anodes based on ion adsorption/desorption should be adopted. MnO_2 nanorods cathode were coupled with AC anode to fabricate ZIHSCs. The mass ratio of AC to MnO_2 were optimized to be 2.5 to fully utilize both the MnO_2 cathode and AC anode.[6] In order to inhibit the Mn dissolution into the electrolyte, 0.5 M $MnSO_4$ was added into the 2 M $ZnSO_4$ aqueous electrolyte, improving both the capacity (from 54.1 mAh/g to 83.8 mAh/g) and energy density (34.8 Wh/kg to 58.6 Wh/kg), as well as the cycling stability (from 65.3% (3000 cycles) to >60% (5000 cycles)).[6] MnO_2-CNT freestanding paper was employed as cathode to couple with capacitor-type $Ti_3C_2T_x$ MXene paper anode for ZIHSCs.[2c] In the cathode, CNTs to MnO_2 mass ratio was optimized to be 4:3. At loading mass of 1.671 mg, the freestanding MXene paper manifested similar capacitance to the MnO_2-CNT cathode. The MnO_2-CNT//$Ti_3C_2T_x$ based ZIHSC delivered high specific capacitance of 115.1 F/g in 2 M $ZnSO_4$ (with 0.1 M $MnSO_4$) aqueous electrolyte, high energy density of 98.6 Wh/kg and good cycling stability with capacitance retention of 83.6% after 15000 cycles. $MnSO_4$ was also added in the electrolyte to inhibit Mn dissolution.[2c] Pre-intercalation into the tunnel structure of δ-MnO_2 was found out to be effective in improving the electrochemical performance.[7a] Mai et al. successfully incorporated Zn ion pre-intercalation into MnO_2 through hydrothermal reaction, forming Zn_xMnO_2 (α-MnO_2) nanowires in which Mn^{3+} and Mn^{4+} coexisted with presence of Zn^{2+}. By replacing δ-MnO_2 with Zn_xMnO_2 cathode, the ZIHSC demonstrated smaller charger transfer resistance and faster ion diffusion. As shown in Figure 3(e-f), in 2 M $ZnSO_4$ (with 0.4 M $MnSO_4$) aqueous electrolyte, higher areal capacity (1745.8 mF/cm^2 at 2 mA/cm^2) and rate performance (~500 mF/cm^2 at 20 mA/cm^2) and better cycling stability was attained in ZIHSCs constructed with Zn_xMnO_2 cathode than in ZIHSCs with MnO_2 cathode, with activated carbon cloth (ACC) as the anode.[7a]

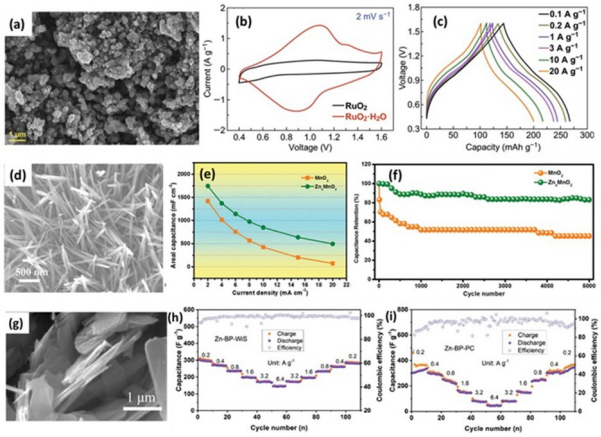

Figure 3. a) SEM image of $RuO_2{\cdot}H_2O$ powder. b) CV curves of $RuO_2{\cdot}H_2O$ and anhydrous RuO_2 at scan rate of 2 mV/s. c) GCD curves of $RuO_2{\cdot}H_2O$ at different current densities. Reproduced from Ref. [8a] with permission. Copyright 2019, The Authors. d) SEM image of Zn-ion pre-intercalated Zn_xMnO_2 nanowires. e) specific capacity at different current densities and f) cycling stability of Zn_xMnO_2 nanowires and MnO_2 nanosheets. Reproduced from Ref. [7a] with permission. Copyright 2020, Wiley-VCH. g) SEM image of few-layer phosphorene. Specific capacity of FL–P//Zn ZIHSCs at different current densities in h) WiS electrolyte and i) PC-based electrolyte. Reproduced from Ref. [31] with permission. Copyright 2020, Wiley-VCH.

2.2.3. Phosphorenes

By cathodic delamination, few-layer phosphorene (FL–P) was prepared as shown in Figure 3(g).[31] The electrochemical performance of ZIHSCs based on FL–P//Zn was evaluated in different electrolytes, one is "water in salt (WiS)" aqueous electrolyte (21 M LiTFSI + 1 M $Zn(CF_3SO_3)_2$), the other one is organic electrolyte (0.2 M $ZnCl_2$ in Et_4NBF_4 (tetraethylammonium tetrafluoroborate)/PC (propylene carbonate)). The voltage window in WiS electrolyte is 0.8–2.2 V (higher voltage will result in lower coulombic efficiency), while larger voltage window of 0.8–2.5 V is attainable in organic electrolyte. As shown in Figure 3(h–i), specific capacitance of 304 F/g (0.2 A/g) and 145.9 F/g (6.4 A/g) can be obtained in WiS electrolyte, with no obvious capacitance decay after 5000 cycles. In organic electrolyte, high capacitance of 363.9 F/g can also be obtained at low current density of 0.2 A/g, yet only 46.1 F/g is retained at 6.4 A/g, with limited cycling stability (< 50% retention after 9500 cycles). The inferior rate performance in organic electrolyte was ascribed to the lower ionic conductivity.[31]

2.2.4. Organic Polymers

Aside from carbon materials and inorganic metal oxides/carbides, or phosphorene, redox-active polymer materials can also be employed as electrodes for ZIHSCs. Flexible carbon cloth was activated through air calcination, resulting in porous carbon cloth (PCC) with oxygen-containing groups, better hydrophilicity and higher SSA.[34] PCC was used as the substrate for subsequent hydrothermal polymerization of poly-dopamine (PDA). PDA with abundance of carbonyl groups was adopted as redox-active cathodes for ZIHSCs. Compared to bare PCC substrates, PDA@PCC manifested better charge storage capability with incorporation of both redox reactions (Zn^{2+}-quinone group coordination) and adsorption-based reactions. At 1 mA/cm^2, PDA@PCC delivered specific capacity of 1.25 mAh/cm^2 and maintained 0.58 mAh/cm^2 at 10 mA/cm^2 in 2 M $ZnSO_4$ aqueous electrolyte, while PCC only demonstrated 0.7 mAh/cm^2 at 1 mA/cm^2 and 0.46 mAh/cm^2 at 10 mA/cm^2.[34]

Most of the above-mentioned ZIHSCs are based on metal Zn anode, which undergoes stripping/deposition and formation of dendrites upon extended cycling. Zn dendrites with high Young's modulus (108 GPa) might pierce through separator and finally lead to device failure.[35] Porous organic polymer-tetra(4-aminophenyl)porphyrin-1,4,5,8-naphthalenetetracarboxylic dianhydride (POP-TAPP-NTCA) microspheres were developed to replace the Zn metal anode in ZIHSCs.[35] The POP-TAPP-NTCA microspheres electrode showed broad redox peaks in CV curves and slopes in GCD profiles vs Zn, due to the reversible Zn-ion storage on carbonyl groups as well as the irreversible Zn-ion storage on porphyrin nitrogen sites.[35] By coupling with capacitor-type exfoliated graphene/polyaniline cathode, ZIHSCs using 2 M $ZnSO_4$ aqueous electrolyte were fabricated with capacitance of 172 F/g at 0.13 A/g and 94 F/g at 1.5 A/g.

The electrochemical performance of the above-discussed carbon-based cathodes (summarized in Table 1) and non-carbon cathode materials (summarized in Table 2) for ZIHSCs have been plotted for a better comparison as shown in Figure 4. Note that the unit of specific capacity for all the ZIHSCs have been converted to mAh/g based on the data provided in respective literature. It can be seen from Figure 4(a) that compared to commercial AC and YP-50F, the approaches discussed in Section 2.1 are quite effective in improving the electrochemical performance of ZIHCSs based on carbon cathodes, reaching ~200 mAh/g at low current density, and some of the carbon cathodes can maintain ~100 mAh/g at high current density of 20 A/g. However, it should be noted that the calculation of specific capacity for most of the carbon cathode is only based on the loading mass of the carbon materials, excluding the heavy weight of bulk Zn metal anode. Thus, the actual capacity of ZIHSCs will be compromised if the weight of the Zn metal anode is included. For ZIHSCs based on non-carbon cathode materials shown in Figure 4(b), overall the specific capacity still hardly reach 200 mAh/g at low current density, except for the V_2CT_x based ZIHSCs due to the delamination and phase change.[9] More efforts are still needed to further increase the capacity and energy density of ZIHSCs.

The borderline between ZIHSCs and Zin-ion batteries (ZIBs) might be ambiguous and one might doubt whether the above-mentioned Zn-ion based charge storage devices are ZIHSCs or ZIBs. However, the differentiation between ZIBs and ZIHSCs are mostly based on the electrochemical mechanisms in the cathode and anode. In ZIBs, the electrochemical mechanisms in cathode and anode are both battery-like (intercalation/con-

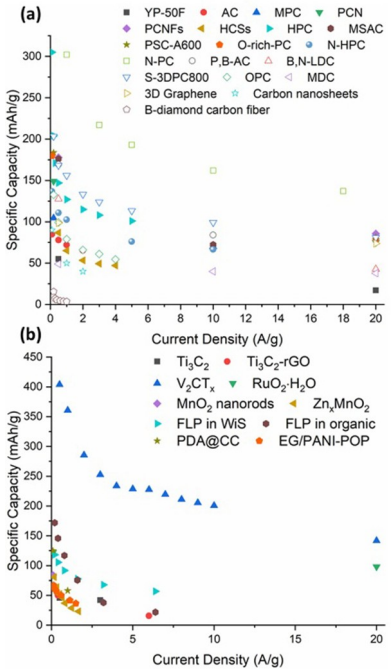

Figure 4. Performance comparison of a) carbon-based electrode materials as listed in Table 1. b) Non-carbon-based electrode materials as listed in Table 2. Note that the unit of specific capacity for all the electrode materials have been converted to mAh/g for better comparison.

Table 1. Electrochemical performance summary of carbon-based cathode materials for ZIHSC.[a]

Materials	Anode	Voltage range [V]	Electrolyte	Capacity	Rate performance	Mass loading	Retention (number of cycles)	Energy density (Power)	Ref.
YP-50F (Kuraray, Japan)	Zn	0.2–1.8	1 M $ZnSO_4$ aq.	55 mAh/g (0.5 A/g)	17.2 mAh/g (20 A/g)	2 mg/cm^2	–	43.1 Wh/kg (12 kW/kg)	[10]
AC	Zn	0–1.8	1 M $Zn(CF_3SO_3)_2$ in AN	170 F/g (0.1 A/g)	131 F/g (2 A/g)	–	91% (20000)	52.7 Wh/kg (17.25 kW/kg)	[7b]
MPC	Zn	0–1.8	1 M $Zn(CF_3SO_3)_2$ in AN	209 F/g (0.2 A/g)	140 F/g (10 A/g)	–	~100% (10000)	92.7 Wh/kg (0.179 kW/kg)	[11]
PCN	Zn	0.1–1.7	1 M $ZnSO_4$ aq.	149 mAh/g (0.2 A/g)	75 mAh/g (20 A/g)	1.6 mg	91% (10000)	119 Wh/kg (0.16 kW/kg)	[12b]
PCNFs	Zn	0.1–1.7	1 M $ZnSO_4$ aq.	177.7 mAh/g (0.5 A/g)	85.5 mAh/g (20 A/g)	1.2 mg	90% (10000)	142.2 Wh/kg (0.4 kW/kg)	[12a]
HCSs	Zn	0.15–1.95	2 M $ZnSO_4$ PAM hydrogel	86.8 mAh/g (0.5 A/g)	47.1 mAh/g (4 A/g)	1.0–1.2 mg/cm^2	98% (15000)	59.7 Wh/kg (0.448 kW/kg)	[13]
HPC	Zn	0.01–1.8	2 M $ZnSO_4$ + 1 M Na_2SO_4 aq.	204 mAh/g (0.2 A/g)	101 mAh/g (5 A/g)	0.9 mg/cm^2	94.9% (2000)	118 Wh/kg (~0.2 kW/kg)	[16]
MSAC	Zn	0.3–1.8	2 M $ZnSO_4$ aq.	176 mAh/g (0.5 A/g)	72.3 mAh/g (10 A/g)	0.9 mg/cm^2	78% (40000)	188 Wh/kg (0.533 kW/kg)	[17]
PSC-A600	Zn	0.2–1.8	1 M $Zn(CF_3SO_3)_2$	183.7 mAh/g (0.2 A/g)	81.8 mAh/g (20 A/g)	2 mg/cm^2	92.2% (10000)	147 Wh/kg (0.136 kW/kg)	[18]
O-rich PC (PC700)	Zn	0–1.9	3 M $Zn(ClO_4)_2$ aq.	179.8 mAh/g (0.1 A/g)	78.4 mAh/g (20 A/g)	1.4-2.0 mg/cm^2	99.2% (20000)	104.8 Wh/kg (0.0585 kW/kg)	[19]
N-HPC	Zn	0.2–1.8	2 M $ZnSO_4$ aq.	136.8 mAh/g (1 A/g)	66.5 mAh/g (10 A/g)	1 mg/cm^2	90.9% (5000)	191 Wh/kg (0.058 kW/kg)	[21]
N-PC	Zn	0.15–1.7	2 M $ZnSO_4$ aq.	302 mAh/g (1 A/g)	137 mAh/g (18 A/g)	1.1 mg/cm^2	>100% (10000)	157.6 Wh/kg (0.69 kW/kg)	[22]
P,B-AC	Zn	0.2–1.8	2 M $ZnSO_4$ aq.	169.4 mAh/g (0.5 A/g)	84 mAh/g (10 A/g)	–	88% (30000)	169.4 Wh/kg (0.5 kW/kg)	[14]
B, N-LDC	Zn	0.2–1.8	1 M $ZnSO_4$ aq.	127.2 mAh/g (0.5 A/g)	42.8 mAh/g (20 A/g)	2 mg/cm^2	81.3% (6500)	86.8 Wh/kg (12.2 kW/kg)	[10]
S-3DPC	Zn	0.2–1.8	2 M $ZnSO_4$ aq.	203.3 mAh/g (0.2 A/g)	81 mAh/g (20 A/g)	5 mg	96.8% (18000)	162.6 Wh/kg (0.16 kW/kg)	[20a]
Oxidized CNT	Zn	0–1.8	1 M $ZnSO_4$ aq. PVA	20 mF/cm^2 (10 mV/s)	8.5 mF/cm^2 (500 mV/s)	–	–	–	[23]
CNT (O plasma treated)	Zn	0.2–1.8	1 M $ZnSO_4$ aq. gelatin	83.2 mF/cm^2 (1 mA/cm^2)	65 mF/cm^2 (10 mA/cm^2)	–	87.4% (6000)	29.6 μWh/cm^2 (0.8 mW/cm^2)	[24]
OPC	Zn	0.2–1.8	1 M $ZnSO_4$ gel electrolyte	132.7 mAh/g (0.2 A/g)	54.5 mAh/g (4 A/g)	0.8–1.2 mg/cm^2	87.6% (10000)	82.36 Wh/kg (~0.11 kW/kg)	[25]
MDC	Zn	0.1–1.7	1 M $ZnSO_4$ aq.	~120 F/g (0.2 A/g)	48 mAh/g (500 A/g)	–	99% (20000)	36.4 Wh/kg (~0.11 kW/kg)	[26]
3D graphene	Zn	0.2–1.8	1 M $ZnSO_4$ aq.	222.03 F/g (0.5 A/g)	166.25 F/g (20 A/g)	–	80% (30000)	118.42 Wh/L (–)	[27]
Carbon nanosheets	Zn	0–1.8	1 M $ZnSO_4$ aq.	~90 mAh/g (0.1 A/g)	~50 mAh/g (2 A/g)	1 mg	90.9% (4000)	75.22 Wh/kg (0.036 kW/kg)	[5d]
rGO/CNT fiber	Zn	0–1.8	2 M $ZnSO_4$ PAA hydrogel	104 F/cm^3 (0.4 A/cm^3)	76.7 F/cm^3 (8 A/cm^3)	–	98.3% (10000)	48.5 mWh/cm^3 (~0.2 kW/cm^3)	[28]
B-diamond/ carbon fiber	Zn	0.2–1.8	1 M $ZnSO_4$ aq.	35.1 F/g (0.2 A/g)	8.1 F/g (1 A/g)	–	89.9% (10000)	70.7 Wh/kg (0.709 kW/kg)	[29]
Graphite	Zn	0–1.8	1 M $Zn(OAc)_2$ ([Ch] OAc + 30 wt.% H_2O)	~144.4 F/g (0.2 A/g)	–	1 mg/cm^2	86% (1000)	52.6 Wh/kg (0.145 kW/kg)	[30]

[a] PC: porous carbon, AC: activated carbon, MPC: mesoporous carbon, PCN: porous carbon nanosheets, PCNFs: porous carbon nanoflakes, HCSs: hollow carbon spheres, HPC: hierarchical porous carbon, MSAC: mesoporous structured activated carbon, PSC-A600: pencil-shavings derived carbon activated at 600 °C, LDC: layered B, N co-doped porous carbon, : MDC: MOF-derived carbon.

version). Nonetheless, in ZIHSCs the electrochemical mechanisms in cathode and anode are different, one is battery-like (intercalation/conversion) while the other one is normally capacitive (physical adsorption/desorption) dominated. In addition, sharp redox peaks in CV and obvious plateaus in GCD profiles are normally found only in ZIBs, which should be absent in ZIHSCs.

3. Electrochemical Mechanism Understanding in ZIHSCs

As categorized in section 2.1 and 2.2, carbon materials have been applied as cathode materials for ZIHSCs with Zn metal as the anode, while non-carbon based materials are also employed to couple with different counter electrode to construct ZIHSCs. The charge storage mechanism for the two electrodes in ZIHSCs are generally different, one is based on adsorption/desorption, the other is based on redox-active reactions. However, the detailed electrochemical mechanism of

Table 2. Electrochemical performance summary of non-carbon-based cathode materials for ZIHSC.[a]

Materials	Anode	Voltage range [V]	Electrolyte	Capacity	Rate performance	Mass loading	Retention (number of cycles)	Energy density	Ref.
Ti_3C_2	Zn@Ti_3C_2	0.1–1.35	1 M $ZnSO_4$ + gelatin	132 F/g (0.5 A/g)	121 F/g (3 A/g)	–	82.5% (1000)	–	[32]
$Ti_3C_2T_x$-rGO aerogel	Zn	0.2–1.6	2 M $ZnSO_4$	128.6 F/g (0.4 A/g)	40.3 F/g (6 A/g)	1 mg	95% (75000)	34.9 Wh/kg (0.28 kW/kg)	[33]
V_2CT_x	Zn	0.1–2	21 M LiTFSI + 1 M Zn-$(CF_3SO_3)_2$	508 mAh/g (0.2 A/g)	141.8 mAh/g (20 A/g)	1–1.5 mg	>100% (18000)	386.2 Wh/kg (–)	[9]
				765.47 F/g (0.2 A/g)	268.67 F/g (20 A/g)				
$RuO_2{\cdot}H_2O$	Zn	0.4–1.6	2 M $Zn(CF_3SO_3)_2$	122 mAh/g (0.1 A/g)	98 mAh/g (20 A/g)	2.5–3 mg/cm^2	87.5% (10000)	119 Wh/kg (~0.1 kW/kg)	[8a]
MnO_2 nanorods	AC	0–2	2 M $ZnSO_4$ + 0.5 M $MnSO_4$	83.8 mAh/g (0.1 A/g)	–	–	~61.8% (5000)	58.6 Wh/kg	[6]
			2 M $Zn(CF_3SO_3)_2$	46.4 mAh/g (0.1 A/g)			93.4% (2000)	29.5 Wh/kg	
MnO_2-CNTs	$Ti_3C_2T_x$ MXene	0–2	2 M $ZnSO_4$ + 0.1 M $MnSO_4$	115.1 F/g (1 mV/s)	67.5 F/g (20 mV/s)	1.671 mg (anode)	83.6% (15000)	98.6 Wh/kg (0.078 kW/kg)	[2c]
Zn_xMnO_2 nanowires	AC cloth	0–2	2 M $ZnSO_4$ + 0.4 M $MnSO_4$	1745.8 mF/cm^2 (2 mA/cm^2)	~500 mF/cm^2 (20 mA/cm^2)	12 mg/cm^2	83.1% (5000)	969.9 μWh/cm^2 (~2 mW/cm^2)	[7a]
				145.48 F/g (0.167 A/g)	41.67 F/g (1.67 A/g)				
Few-layer phosphorene	Zn	0.8–2.2	21 M LiTFSI + 1 M Zn-$(CF_3SO_3)_2$	304 F/g (0.2 A/g)	145.9 F/g (6.4 A/g)	0.6–0.8 mg/cm^2	>95% (5000)	204.4 Wh/kg (~0.6 kW/kg)	[36]
		0.8–2.5	2 M $ZnCl_2$ (in Et_4NBF_4/PC)	363.9 F/g (0.2 A/g)	46.1 F/g (6.4 A/g)	0.6–0.8 mg/cm^2	~43% (9500)	315.6 Wh/kg (~0.7 kW/kg)	
PDA@PCC	Zn	0.1–1.8	2 M $ZnSO_4$	1.25 mAh/cm^2 (1 mA/cm^2)	0.58 mAh/cm^2 (10 mA/cm^2)	9–10 mg/cm^2	100% (10000)	1.06 mWh/cm^2 (0.85 mW/cm^2)	[34]
EG/PANI	POP-TAPP-NTCA	0.1–1.5	2 M $ZnSO_4$	172 F/g (0.13 A/g)	94 F/g (1.5 A/g)	1–1.22 mg/cm^2	90% (1100)	48 Wh/kg (0.085 kW/kg)	[35]

[a] PDA: poly-dopamine, PCC: porous carbon cloth, EG: ethylene glycol, PANI: polyaniline, POP-TAPP-NTCA: porous organic polymer-tetra(4-aminophenyl) porphyrin-1,4,5,8-naphthalenetetracarboxylic dianhydride.

different electrode materials in ZIHSCs remain unclear. In this section, efforts to unveil the charge storage mechanism of ZIHSCs based on carbon and non-carbon cathodes are discussed and summarized.

Activated carbon (AC) was employed as cathode to couple with Zn for the assembly of ZIHSCs with aqueous $ZnSO_4$ electrolyte. Through SEM and XRD analysis on both cathode and anode at different charge/discharge states, it was found out that there is $Zn_4SO_4(OH)_6{\cdot}5H_2O$ formed on the Zn surface, due to unstable pH value in the electrolyte during charge/discharge processes. The Zn surface is also getting rougher along with cycling, with different Zn crystal orientation. For the AC cathode, adsorption of both Zn^{2+} and SO_4^{2-} also leads to formation of $Zn_4SO_4(OH)_6{\cdot}5H_2O$ particles on the surface, without affecting the phase composition and morphology of AC electrode. Thus, the energy storage mechanism in this ZIHSC is primarily based on physical ion adsorption on the cathode, and Zn^{2+} plating/stripping at the anode, accompanied by formation/dissolution of $Zn_4SO_4(OH)_6{\cdot}5H_2O$ on both cathode and anode.[36]

Electrochemical mechanism of ZIHSCs based on PSC-600 obtained through activation of pencil derived porous carbon has been studied. With ex-situ X-ray diffraction, it was found out that the diffraction peak of PSC-600 remained unchanged during the charge/discharge process, indicating the physical adsorption/desorption dominant mechanism. However, presence of $Zn(CF_3SO_3)_2[Zn(OH)_2]_3{\cdot}xH_2O$ was also confirmed in combination with energy dispersive spectroscopy (EDS). The varied Zn and F content at different charge/discharge states indicates the likely formed $Zn(CF_3SO_3)_2[Zn(OH)_2]_3{\cdot}xH_2O$ during the charge process, partially decomposed during discharge.[18] The electrochemical mechanism of carbon nanosheets cathode was investigated by multiple ex-situ characterization methods.[5d] At the discharged state, the surface pore density reduction was evidenced by SEM observation, which is ascribed to the Zn-ion adsorption. Higher Zn atomic ratio at the discharged state was also quantified through EDS mapping. Ex-situ Raman spectra revealed a smaller I_D/I_G ratio at the discharged state with red-shifted G band, due to the interaction of adsorbed Zn ions with the carbon nanosheets that resulted in a lower defect degree. Higher C–O–Zn/C–OH bonding ratio at the discharged state was evidenced through ex-situ XPS of the C1s spectra. Thus, the electrochemical mechanism of carbon nanosheets was related to the reversible Zn-ion adsorption/desorption at low voltage.[5d] However, at high voltage region (charged state), it is likely that the anions in electrolyte are also adsorbed on the surface of the carbon nanosheets. Also, in aqueous $ZnSO_4$ electrolyte, it is likely that

there is $Zn_4SO_4(OH)_6 \cdot 5H_2O$ formation on the carbon cathode during charge/discharge process.[36]

As discussed in section 2.1.3, expanding the voltage window (from 0.5–1.5 V to 0–1.9 V) can increase the capacitance of PC800 through incorporation of reversible hydrogen adsorption/desorption (~0–0.2 V) and reversible oxidation/reduction of surface carbon atoms or oxygen functional groups (~1.7–1.9 V).[8b] As shown in Figure 5(a), the morphology of PC800 remains unchanged before being discharged to 0 V.

However, when being discharged to 0 V, formation of nanosheets on the surface was noticed, which were verified to be alkaline salts of $Zn_4ClO_4(OH)_7$ and $Zn(OH)_2$ as shown in the XRD pattern of discharged PC800 in Figure 5(c). In-situ XRD pattern of PC800 displayed in Figure 5(d) also confirmed the formation of zinc alkaline salts on PC800 at low potential (0–0.25 V). The formation of alkaline salts was attributed to the hydrogen adsorption at discharged state that resulted in a local alkaline environment on the surface of PC800. Upon anodic reaction, as shown in Figure 5(b), the carbonyl content (C=O) in PC800 was found to increase from 16.9% to 44.3% when being charged from 0.76 V to 1.9 V, and restored back to 17.5% when discharged to 0.76 V.[19] Thus, the electrochemical mechanism of PC800 in ZIHSCs was based on reversible hydrogen adsorption/desorption at low voltage and reversible oxidation/reduction of surface carbonyl groups at high voltage.

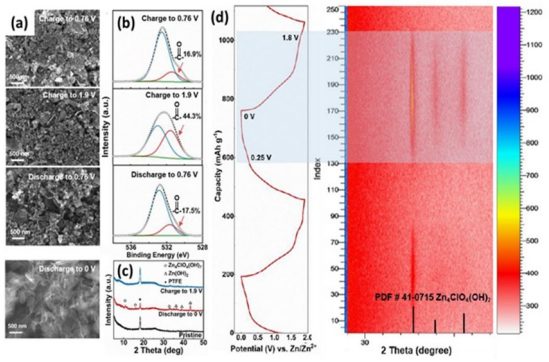

Figure 5. a) SEM image, b) C1s XPS spectra, and c) Ex-situ XRD patterns of PC800 at different charge/discharge states. d) In-situ XRD patterns of PC800. Reproduced from Ref. [8b] with permission. Copyright 2020, Wiley-VCH.

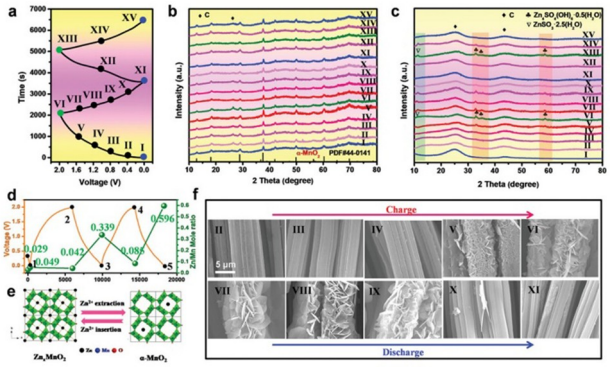

Figure 6. Electrochemical mechanism investigation of ZIHSCs based on Zn_xMnO_2 cathode and ACC anode. a) GCD curves of ZIHSC at 2 mA/cm^2. The corresponding ex-situ XRD pattern of b) Zn_xMnO_2 cathode and c) ACC anode. d) The change of the Zn/Mn molar ratio in Zn_xMnO_2 cathode during charge/discharge. e) Schematic illustration of the zinc storage mechanism in the Zn_xMnO_2 electrode. f) SEM images of the ACC at charge/discharge states. Reproduced from Ref. [7a] with permission. Copyright 2020, Wiley-VCH.

Unlike carbon cathodes that mostly rely on physical adsorption/desorption, the electrochemical mechanism of ZIHSCs based on MnO_2 cathode and AC anode is different. ZIHSCs based on Zn-ion pre-intercalated Zn_xMnO_2 cathode demonstrated higher charge storage capability than ZIHSC based on bare δ-MnO_2 as discussed in Section 2.2, when coupled with ACC anode.[7a] Electrochemical mechanisms of Zn_xMnO_2 cathode and ACC anode were investigated with different ex-situ methods as shown in Figure 6. As displayed in Figure 6(b), the crystal structure of Zn_xMnO_2 remain unchanged during charge/discharge, without formation of new phases, indicating the good reversibility and stability of the Zn_xMnO_2 cathode. The Zn/Mn ratio in Zn_xMnO_2 cathode at different charge/discharge states were quantified by inductively coupled plasma as shown in Figure 6(d). The Zn/Mn ratio increases along with discharge and decreases along charging of ZIHSC. The Zn/Mn ratio was also increased to 0.596 after 3 cycles of discharge, indicating the Zn intercalation/de-intercalation mechanism in Zn_xMnO_2 cathode with Zn trapping effect as schemed in Figure 6(e). For ACC anode, when ZIHSC was charged, formation of Zn sulfate hydroxide and Zn sulfite were detected as evidenced in Figure 6(b) with formation of nanosheets on the surface as observed by SEM shown in Figure 6(f), which also contributed to the capacity of ZIHSCs.[7a] Similarly, in ZIHSCs constructed by MnO_2 nanorod cathode and AC anode, Zn ion intercalation in MnO_2 was also evidenced with formation of $Zn_{1+x}Mn_3O_7 \cdot 3H_2O$ at discharged state.[6] Partially reversible formation/dissolution of zinc sulfate hydroxide on both MnO_2 nanorod cathode and AC anode were also observed, which was related to the changeable pH value in the electrolyte during charge/discharge.[6]

Till now the reported electrochemical mechanism investigation of ZIHSCs is still limited. More efforts are to be paid for a better understanding. For example, the contribution of the functional groups/dopants in carbon cathodes to the energy storage performance of ZIHSCs are still not well understood. The variation of oxidation state, coordination chemistry and crystal structure, etc. of those non-carbon based cathodes during Zn ion storage are to be further analyzed. Understanding of the formation process of Zn dendrites/byproducts on the electrode and their effect on the performance of ZIHSCs are still lacking. Also, it should be noted that in-situ methods are favorable than ex-situ methods for electrochemical mechanism investigation, as in-situ methods are capable of capturing intermediate phases/products during the dynamic electrochemical reactions.[1d,37]

4. Zn Anode in Aqueous Electrolytes for ZIHSCs

Benefitting from the merits of low redox potential (−0.76 V vs SHE), good tolerance to air and humidity, and high theoretical gravimetric and volumetric capacity, metallic Zn (such as Zn foil

and Zn nanostructures) can be directly utilized as stable battery-type anode in aqueous electrolytes for ZIHSCs. The fast adsorption/desorption of electrolyte ions into/from highly porous cathode materials combined with good ionic conductivity of aqueous electrolytes contribute to the improved kinetics, rate capability and power density of ZIHSCs. Thus, the high-rate power supply of ZIHSC is predominantly determined by the diffusion-controlled Zn stripping/deposition process at anode side. However, heterogeneous nucleation of Zn deposition and subsequent Zn dendrite growth is one critical issue resulting into the failure of ZIHSCs, especially when high current densities are applied to achieve desirable power densities. Additionally, side reactions and Zn corrosion would lead to poor irreversibility, low coulombic efficiency and short cycle life of ZIHSCs. Therefore, in this section, the issues at the Zn side in ZIHSCs would be presented, followed by the corresponding strategies.

4.1. Issues of Zn Anode in Aqueous Electrolytes for ZIHSCs

4.1.1. Zn Dendrite Formation and Growth

It is well known that Zn dendrite formation and growth would severely affect the cycling performance and possibly lead to short circuit and battery failure during operation when separators are pierced by dendrites. It is reported that Zn dendrite formation and growth in alkaline electrolytes (such as KOH, NaOH and LiOH-containing solutions with $Zn(Ac)_2$) is more severe than that in mildly acid and neutral electrolytes (Figure 7a).[38] It can be attributed to the generation of $Zn(OH)_4^{2-}$ ions when metallic Zn anode is oxidized in alkaline mediums. Furthermore, $Zn(OH)_4^{2-}$ species are also formed due to Zn self-corrosion process in alkaline electrolytes. When $Zn(OH)_4^{2-}$ ions are saturated in the solutions, they tend to decompose into inert ZnO layer on the surface of Zn anode, thus blocking the subsequent ion diffusion and deposition and reducing electrochemically active surface area. Additionally, apparent shape change and uneven surface morphology of Zn anode would occur as a result of Zn self-corrosion process in alkaline solutions.[39] $Zn(OH)_4^{2-}$ ions preferentially diffuse to protrusions with large curvature radius, where localized current density is strengthened. The inhomogeneous distribution of $Zn(OH)_4^{2-}$ ions near Zn surface, accumulation of $Zn(OH)_4^{2-}$ ions on the protrusions and uneven current distribution over the Zn anode consequently speeds up dendrite formation in alkaline electrolytes during repeated Zn plating/stripping processes, resulting in irreversibility and fast capacity decay. 1D branch-like topologies of Zn dendrites are commonly observed in alkaline electrolytes, even under moderate operation conditions, such as low current densities and low areal capacities.[40] These 1D dendrites are more likely to pierce separators and cause short circuit and failure of ZIHSC.

By contrast, Zn dendrites in mildly acid/neutral electrolytes are negligible/alleviated at low current densities (<2 mA/cm^2) and areal capacities (0.5 mAh/cm^2).[5c,41] Besides, 2D hexagonal morphologies of Zn dendrites in mildly acid/neutral electrolytes

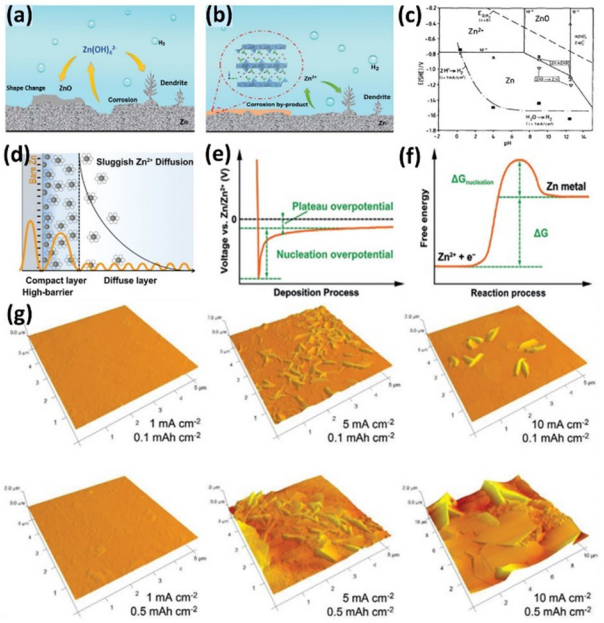

Figure 7. a) Schematic illustration of Zn electrode issues in alkaline electrolytes. b) Schematic presentation of Zn electrode issues in mildly acid/neutral electrolytes. The inset shows the hexagonal byproduct of $Zn_4SO_4(OH)_6 \cdot H_2O$ in 1 M $ZnSO_4$. (a–b) Reproduced from Ref. [38a] with permission. Copyright 2020, The Royal Society of Chemistry. c) Pourbaix diagram of Zn/H_2O system with 10^{-4} M Zn^{2+}. Reproduced from Ref. [38e] with permission. Copyright 1991, Elsevier. (d) Electric double layer structure in the vicinity of Zn anode. The yellow line indicates the corresponding energy barrier. Reproduced from Ref. [44] with permission Copyright 2020, The Royal Society of Chemistry. e) Voltage profile during zinc deposition. f) Energy barrier during zinc nucleation process. (e–f) Reproduced from Ref. [45] with permission. Copyright 2020, Wiley-VCH. g) AFM images of Zn deposits under different current densities and areal capacities. Reproduced from Ref. [41b] with permission. Copyright 2019, Wiley-VCH.

weaken their capability to pierce separators. Therefore, mildly acid and neutral electrolytes are preferentially utilized in ZIHSCs, such as $ZnSO_4$, $Zn(CF_3SO_3)_2$ and $Zn(TFSI)_2$, which display wide electrochemical window, high ionic conductivity and good reversibility of Zn stripping/plating. While for other mild electrolytes like $Zn(NO_3)_2$, the oxidizing property of NO_3^- lead to rapid Zn oxidation and poor coulombic efficiency, thus they are not employed in ZIHSCs. However, it should be noted that Zn dendrite formation and growth in mildly acid/neutral electrolytes still remains a huge challenge for ZIHSCs with high charge/discharge rate and desirable rate capability and power/energy density.[42] It is because that high current densities/areal capacities incur large amounts of dendrite nucleation and large-sized dendrites, which would rapidly deteriorate reversibility, decrease capacity, aggravate the piercing of separators and paralyze ZIHSCs.

In mildly acid/neutral electrolytes, Zn^{2+} ions are the charge carriers. Smooth surface morphology of Zn anode and uniform electric field contribute to homogeneous diffusion and deposition of Zn^{2+} ions.[43] The concentration gradient of Zn^{2+} ions near the surface of Zn anode also influences dendrite formation and growth, illustrated from an electrical double layer model (Figure 7(d)).[44] Driven by electric force, Zn^{2+} ions would continuously transport to the diffusion layer and then reduction

of Zn^{2+} takes place at active sites to form a deposited Zn layer, where Zn^{2+} concentration gradient occurs. The uniformity of the deposited layer is highly dependent on the nucleation and plateau overpotential (Figure 7(e–f)).[45] The larger current densities, the higher overpotential and the severer concentration polarization, thus leading to inhomogeneous Zn^{2+} diffusion and deposition of Zn dendrites. These dendrites/protrusions with higher curvature ratio would attract and accumulate more Zn^{2+} ions due to higher electric field, further aggravating Zn dendrite formation and growth during long-term cycling. Therefore, strategies, such as modifications of electrode surface, introduction of electrolyte additives and electrode structure design, will be discussed later to efficiently homogenize ionic flow and electron distribution to mitigate Zn dendrites.

4.1.2. Zn Metal Corrosion

Zn metal corrosion is another critical issue in aqueous electrolytes for ZIHSC. Unlike the byproducts of $Zn(OH)_2$ and inert ZnO layer in alkaline systems during Zn corrosion, hexagonal $Zn_4SO_4(OH)_6 \cdot H_2O$ and $TFSI^-$-based complexes would be generated as byproducts on the surface of Zn anode in mild electrolytes of 1 M $ZnSO_4$ and $Zn(TFSI)_2$, respectively (Figure 7(b)).[46] However, these byproducts from Zn corrosion in mildly acid/neutral electrolytes are loose, allowing electrolytes to continuously contact with fresh Zn anode. It indicates unceasing Zn corrosion reactions and constant consumption of Zn electrode and electrolytes, resulting in limited shelf life of ZIHSCs. Additionally, uneven surface morphology resulted from Zn corrosion would inevitably incur dendrite growth and formation and lower coulombic efficiency. Another problem from Zn corrosion is H_2 evolution when Zn react with $ZnSO_4$ or $Zn(TFSI)_2$ mild electrolytes.[47] The H_2 evolution would be the cause of swelling, increased internal pressure or even explosion for sealed ZIHSCs. It is reported that ~19.8 μL of aqueous electrolytes was consumed, ~15.9 mAh of Zn was deactivated and ~6.7 mL of H_2 gas was accordingly generated in a Zn symmetric pouch cell with Zn metal size of 4×4 cm^2 and 3 M $ZnSO_4$ after a dwell time of 4 weeks.[48] Thus, it is of significance to improve chemical resistivity of Zn electrode for practical applications of ZIHSCs.

4.2. Strategies to Regulate Uniform Zn Plating/Stripping

4.2.1. Zn Electrode Design

Compared to commercial Zn foil, 3D conductive Zn networks are reported to remarkably shorten ion diffusion path, provide abundant active sites, lower localized current density and homogenize localized electrical field to facilitate kinetics and lower overpotential of diffusion-controlled Zn stripping/deposition process and suppress Zn dendrites during long-term cycling.[49] Owing to chemical and electrochemical stability, high electrical conductivity and robust mechanical strength, various 3D porous substrates, such as carbon fiber/cloth and nickel foam, are selected as current collectors for Zn deposition in ZIHSCs. For example, hierarchically nanostructured Zn electrodes were electrodeposited on nickel foam and carbon fiber for flat-type and fiber-type ZIHSC (Figure 8(a–c)), respectively, with activated carbon as cathode and PVA/$ZnSO_4$ as gel electrolytes.[50] A high energy density of 208 Wh/kg and a high power density of 20 kW/kg as well as excellent cyclability over 10000 cycles at a current density of 20 A/g were achieved in flat-type ZIHSC. A high areal energy density of 25 μWh/cm^2, a high areal power density of 3000 μW/cm^2, excellent cycling stability (over 10000 cycles), outstanding mechanical flexibility and good water-proof property were exhibited in fiber-type ZIHSC. These promising results could be attributed to short ion diffusion length and large electrochemical active surface area with reduced Zn nucleation size and lower nucleation and growth overpotential.

Graphite fibers were also selected as substrates for the electrodeposition of layered Zn sheets (Figure 8(d-e)).[51] Quasi-solid-state fiber-shaped ZIHSC was then assembled with the prepared graphite/Zn fiber as battery-type negative electrode, high surface-area and conductive reduced graphene oxide/carbon nanotube composite fiber as capacitor-type positive electrode and high ionic-conductivity $ZnSO_4$/polyacrylic acid hydrogel as gel electrolyte. The integrated ZIHSC delivered a high energy density of 48.5 mWh/cm^3, a high power density of 3600 mW/cm^3 and excellent capacity retention of 98% after 10000 cycles at a current density of 3.2 mA/cm^3. Minor morphology and shape change and no dendrite formation were observed at negative electrode after cycling at fast charge/discharge rates (Figure 8(f–h)). It could also be attributed to abundant active sites of layered graphite/Zn composite fiber to facilitate and regulate ion transport and reduce Zn

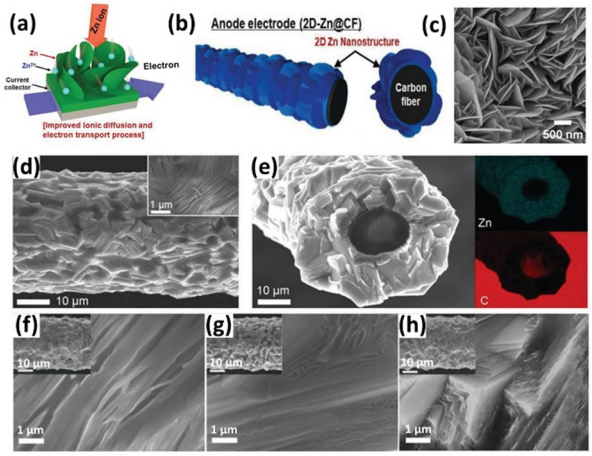

Figure 8. a) Schematic illustration of hierarchically nanostructured Zn metal electrode. b) Schematic illustration of the prepared 3D Zn networks on carbon fibers as anode. c) SEM image of 3D networks on carbon fibers. (a–c) Reproduced from Ref. [50] with permission. Copyright 2020, Wiley-VCH. d) Surface morphology of Zn networks on carbon fibers. e) Cross-section of Zn networks on carbon fibers and the corresponding EDX mapping. SEM images of the prepared Zn networks on carbon fibers as anode in ZIHSC after f) 500, g) 2000, and h) 10000 charge/discharge cycles. Reproduced from Ref. [51] with permission. Copyright 2019, Wiley-VCH.

nucleation/growth size with lower overpotential for reversible Zn stripping/deposition process at high current densities. Other method, like chemical etching of Zn foil to modify surface morphology and enhance surface area, was also employed to shorten ion diffusion pathways and provide increased active sites to achieve enhanced power density and long cycle life of ZIHSCs.[52]

However, Zn affinity has not been taken into consideration when choosing these 3D substrates for Zn plating. For example, carbon-based substrates display poor Zn affinity, as quantified by the low binding energy of −0.34 eV with Zn atom, lower than that between Zn surface and Zn atom (−0.68 eV).[53] It indicates Zn plating continues at the Zn surface rather than carbon substrates after Zn nucleation, thus leading to large Zn nucleation/growth overpotential, uneven Zinc distribution and severe Zn dendrites on carbon-based substrates. Even though nickel foam exhibits large binding energy (−2.09 eV) with Zn atom,[53] its excellent catalytic activity of hydrogen evolution, which is competing with Zn plating, reveals that nickel is also not ideal host for Zn plating. Nevertheless, the hydrogen evolution issue was not investigated in the above assembled ZIHSC. By contrast, copper-based substrates, such as copper mesh[54] and copper foam,[55] demonstrate a high binding energy of −1.58 eV with Zn atom. Additionally, the formation of $CuZn_5$ during nucleation process further enhances the binding energy to −1.94 eV.[53] The superior Zn affinity regulates electrical field, decreases overpotential and promotes uniform Zn deposition. However, the development of ZIHSC is still at its infancy stage and the utilization of copper-based or other substrates for Zn plating has not yet been explored in ZIHSCs. On the other hand, accelerated Zn metal corrosion and gas evolution are overlooked in these nanostructured Zn networks with high surface area. The shelf life/lifespan should also be evaluated in these assembled ZIHSC. Additionally, morphology change at anode side and electrochemical performance of assembled ZIHSCs should be investigated at practical conditions as well as laboratory testing conditions. The minor morphology changes under laboratory testing conditions may be harmless while the morphology can dramatically alter with catastrophic internal short circuit issue under practical conditions. Furthermore, the synthesis complexity of Zn deposition on 3D substrates should also be taken into account as it affects manufacture productivity for large-scale applications.

4.2.2. Zn Surface Modification

Inspired from suppression of Li dendrites and side reactions of solid electrolyte interface (SEI) layer in Li metal batteries, artificial interface layers are constructed at Zn anode to protect Zn from direct contact with electrolytes, alleviate dendrite formation and constrain side reactions.[56] Effective artificial interface layers are generally required to deliver good chemical/electrochemical compatibility with Zn metal and electrolytes, sufficient mechanical strengths to suppress dendrite growth and fast and uniform Zn^{2+} diffusion to Zn anode. Based on different protective strategies, artificial interface layers are divided into three types: carbon-based, inorganic-based and polymer-based interface layers.[57] For example, free-standing and conductive carbon nanotube (CNT) scaffolds were placed on Zn foil during assembling of ZIHSC.[58] The CNT scaffolds could mechanically reduce volume change and constrain Zn dendrites during Zn plating/stripping. The good conductivity and high surface-area of CNT networks guarantee uniform electrical field on Zn surface, thus beneficial to lower polarization voltages, mitigated dendrites and enhanced cycling reversibility (7000 cycles at a moderate current density of 2 A/g) of ZIHSC.

However, Zn plating on conductive CNT scaffolds cannot be avoided, especially at high current densities, indicating morphology change and dendrite formation at CNT networks to pierce separator and induce possible short circuit issue. Furthermore, Zn metal corrosion and side reactions are not solved in the prepared ZIHSC as electrolytes can still pass through the CNT scaffolds to react with Zn anode. Thus, it is preferable to utilize semi-conductive/insulating inorganic or polymer-based interface layers with water resistant capability to shield Zn from attack of bulk electrolytes for ZIHSC applications. Unfortunately, so far, these inorganic or polymer-based interface layers have not yet been investigated in ZIHSCs. In spite of that, we can still gain some knowledge and inspirations from the strategies employed in Zn metal-based batteries. For example, polyamide membrane was selected as the interface layer, contributed to extended lifespan of Zn plating/stripping over 8000 hours with a large areal capacity of 10 mAh/cm^2 at a high current density of 10 mA/cm^2 and prolonged cycling life over 1000 cycles with 88% capacity retention in MnO_2//Zn battery.[47] The excellent electrochemical performance could be attributed to de-solvation of hydrated zinc ions by polyamide membrane, thus suppressing side reactions with enhanced reversibility. Additionally, owing to the coordination of amide groups with Zn^{2+} ions, polyamide membrane could restrict Zn^{2+} diffusion and regulate Zn deposition with dendrite-free Zn anode. Similarly, metal-organic frameworks (MOF) channels were also reported to block large-sized hydrated zinc ion complexes from bulk electrolytes, thus contributing to a super-saturated electrolyte on the surface of MOF-coated Zn anode.[59] Owing to the super-saturated front surface, the Zn symmetric half cells with the MOF-coated Zn exhibited a lifespan up to 3000 hours. Furthermore, because of robust covalent cross-linking networks, these polymer-based interface layers deliver excellent structure stability instead of pulverization during repetitive Zn deposition/stripping.[60] The viscoelasticity of polymer-based layers is beneficial to reversible shape change and guiding transverse Zn deposition.[61] Inorganic interface layer, such as 3D nanoporous ZnO layer, has also been demonstrated to accelerate the kinetics of Zn^{2+} transfer and deposition and reduce side reactions with high reversibility and stability in the assembled MnO_2//Zn battery.[44] It is benefited from the reduced Zn^{2+} insertion energy barrier and electrostatic attraction towards Zn^{2+} rather than hydrated Zn^{2+} complex. Therefore, these above strategies of employing polymer- or

inorganic-based artificial interface layers can also be adopted in ZIHSCs for improved electrochemical performance.

4.2.3. Electrolyte Modification

Electrolyte additives are reported to regulate uniform Zn^{2+} diffusion and deposition, suppress Zn dendrites and inhibit side reactions. For example, the addition of low-cost Na_2SO_4 into $ZnSO_4$ restricted Zn dendrite growth in ZIHSC with enhanced electrochemical performance.[62] It is attributed to the electrostatic shield mechanism, in which Na^+ with high redox potential would anchor at the dendrite sites by the locally enhanced electric field, screen Zn^{2+} at the dendrite sites and repel Zn^{2+} transversely transport to the adjacent planar substrate to restrain Zn dendrite growth and obtain uniform Zn deposition. However, the issues related with Zn metal corrosion, side reactions and generation of H_2 are still not resolved. Increasing salt concentration in the electrolytes is one effective way to decrease free water molecules in the electrolyte to alleviate the above water-induced parasitic reactions. Additionally, because of the decreased free water molecules around Zn^{2+}, energy barrier of desolvation during Zn deposition would accordingly reduce in the concentrated electrolyte, thus improving the kinetics of Zn^{2+} diffusion and deposition. For instance, the water-in-salt type hydrogel filled with 7.5 M $ZnCl_2$ was prepared for ZIHSC with wide electrochemical window, remarkable Zn stripping/plating reversibility and excellent capacity retention of 95% after 100 000 cycles (Figure 9(a–f)).[63] The outstanding electrochemical properties could be attributed to the lower desolvation energy of $[ZnCl]^+(H_2O)n\text{-}1$ (n = 1–6) clusters in the concentrated electrolytes compared to that of $[Zn(H_2O)n]^{2+}$ counterparts in the dilute electrolytes. Furthermore, the reduced size of Zn ions contributed to enhanced energy storage capacity of porous carbon materials at cathode side, thus improving the energy density to battery level of 217 Wh/kg at a power density of 450 W/kg. However, the high concentration would inevitably raise costs and compromise ionic conductivity and rate capability of ZIHSC. Thus, it is recommended to balance electrolyte concentration, device performance and manufacture costs. It is also suggested to explore more salt mixture possibilities by introducing inert cations/anions into electrolytes to improve electrolyte concentration in ZIHSC.

Organic additives into electrolytes, such as polymers and surfactants, have also shown lower corrosion rate and restrained dendrite growth of Zn anode. For example, one cheap surfactant sodium dodecyl benzene sulfonate (SDBS) was introduced as electrolyte additive into MnO_2//Zn batteries.[64] It is evidenced that (100) lattice plane was strengthened compared to (002) lattice plane during Zn plating after introduction of SDBS. This crystal growth orientation change promoted Zn morphology transformation from perpendicular flakes to compact and smooth nanosheets on the surface of Zn anode, thus suppressing dendrite growth. Additionally, the introduction of surfactant SDBS could facilitate interface wettability between aqueous electrolytes and lyophobic Zn anode, thus promoting uniform Zn electroplating. The surfactant SDBS could also absorb on Zn surface and form a passivation layer to protect Zn from corrosion. Tip effect, in which more Zn^{2+} are attracted at the tips due to high electric field, is the main reason for dendrite growth and consequent degraded coulombic efficiency and poor irreversibility. Polarized organic additives, such as diethyl ether,[65] are also promising to inhibit dendrite growth in MnO_2//Zn battery because they are prone to absorb at Zn tips and repel Zn^{2+} attractions. However, the concentration of organic additives needs to optimize as excessive organic additives would decrease electrolyte ionic conductivity, slow down Zn^{2+} diffusion and deposition kinetics and reduce rate capability and power density. As mentioned earlier, the development of ZIHSC is at the early stage. These strategies of organic additives into electrolytes, which have been effective in Zn-based batteries, can be adopted in ZIHSC for enhanced electrochemical performance.

Similarly, gel/solid-state electrolytes can also alleviate Zn metal corrosion and suppress dendrite growth due to the limited H_2O content and the uniform ion distribution and transverse Zn position mediated by polymer additions. One concern of utilizing gel/solid-state electrolytes is their low ion conductivity, which would compromise rate capability and power density of ZIHSCs. Nevertheless, it should be noted that

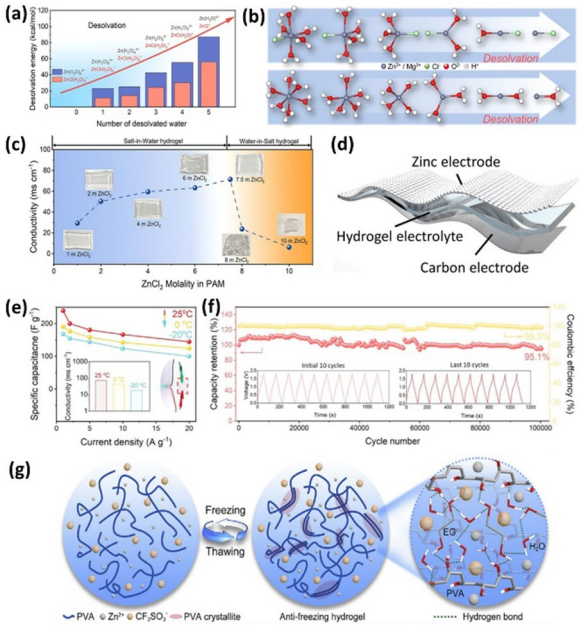

Figure 9. a) Desolvation energies of $[Zn(H_2O)_6]^{2+}$ and $[ZnCl(H_2O)_5]^+$. b) Molecular geometries of the Zn^{2+} and $ZnCl^+$ desolvation processes. c) Ionic conductivity of the hydrogel electrolytes filled with ZnCl2 at different molarities. d) Schematic illustration of the assembled flexible ZISHC. e) Rate capability of the assembled ZIHC at different temperatures. The inset displays the ionic conductivity of the prepared hydrogel electrolyte at different temperatures, and the photo shows the hydrogel electrolyte can serve as ionic conductor to light up an LED. f) Cycling stability of the assembled ZIHSC at a current density of 5 A/g. (a–f) Reproduced from Ref. [63] with permission. Copyright 2020, Wiley-VCH. g) Schematic illustration of the preparation process of anti-freezing hydrogel electrolyte. Reproduced from Ref. [9] with permission. Copyright 2020, Elsevier.

one additional benefit is their multi-functionality, such as flexibility, anti-freezing, self-healing and stretchability, which would be discussed in detail in the following section.

Different from aqueous electrolytes with water as solvent, organic electrolytes are free from water molecules and can avoid water-induced side reactions to improve lifespan.[66] SEI from organic electrolyte decomposition would be formed on Zn surface to mediate Zn^{2+} diffusion and deposition and alleviate Zn dendrites. However, large-sized Zn ion complex in organic electrolytes would lead to large desolvation energy barrier. Low ionic conductivity of organic electrolytes would affect kinetics of redox reactions and impair rate capability and power density. Inert operating environment is also required for organic electrolyte handling and device assembly, resulting in high-cost concern.

5. Physical Properties of ZIHSC

As mentioned earlier, gel/solid-state electrolytes can constrain Zn dendrite growth and alleviate metal corrosion as well as provide multi-functionalities of ZIHSC. For example, undesirable elasticity and ionic conductivity of aqueous-based gel electrolytes under subzero temperatures limit their practical applications. Thus, an anti-freezing gel electrolyte containing poly (vinyl alcohol) (PVA), ethylene glycol (EG), $Zn(CF_3SO_3)$ and H_2O was facilely prepared by repeated freeze/thaw cycles (Figure 9(g)).[9] EG is one effective inhibitor for water freezing because EG can form various molecular clusters with H_2O, disrupt hydrogen bonds between H_2O molecules in the binary solution and reduce saturated vapor pressure of H_2O.[67] The prepared anti-freezing gel electrolyte could maintain unfrozen, good flexibility and a high ionic conductivity of 4.02 mS/cm under a low temperature of −15 °C for a week. The assembled flexible ZIHSC exhibited a high capacity retention of 63.9% at −15 °C compared to the initial capacity measured at ambient temperature of 20 °C.

Flexibility is also desirable for wearable applications. For example, a flexible ZIHSC was prepared based on the zwitterionic natural polymer hydrogel as gel electrolytes.[68] Benefitting from the double network structures formed among sodium alginate (SA), acroleic acid (AA) and acrylamide (AM), the synthesized gel electrolyte could deliver good water retention ability and thus promote high ionic conductivity as well as exhibit acceptable mechanical strength. Outstanding flexibility was demonstrated in the assembled ZIHSC. Stable electrochemical performance was shown at various bending and compressing states. Similarly, polyacrylamide (PAM) hydrogel was prepared for the fabrication of flexible ZIHSC.[13] The assembled flexible ZIHSC could sustain mechanical deformations such as twisting, bending and folding. PVA-based gel electrolyte was also synthesized for flexible ZIHSC.[69] Unfortunately, detailed analysis and investigations of gel electrolytes, electrodes and their interactions are lack in these works.

6. Integrated Systems

It is desirable to combine energy harvester units with energy storage devices as a self-driven integrated systems to power off-grid autonomous devices. It is also highly recommended to develop electrodes of energy storage devices with energy harvesting capability simultaneously, thus avoiding additional external electronics to adjust and match voltage/current output, alleviating interfacial separations among different components, decreasing charge transport resistance, improving energy conversion efficiency and simplifying manufacture process. Owing to the balanced power density and energy density as well as excellent safety and favorable cycling life, ZIHSC are recently proposed to be applied in such self-driven integrated systems.

For example, an air-rechargeable ZIHSC was fabricated consisting of a dual-functional "U" shaped electrode, Zn foil in the middle and two different gel electrolytes sandwiched between "U" shaped electrode and Zn foil (Figure 10(a)).[70] Made from functionalized porous carbon on carbon cloth, the "U" shaped electrode was able to function as capacitor electrode in ZHISC and the air electrode in the Zn-air battery. As air is pervasive, the Zn-air battery could be spontaneously triggered to work and charge ZIHSC by unsealing the tape and exposing air atmosphere to the air electrode (Figure 10(b)). It took ~10 minutes to charge ZIHSC to its 88% with the Zn-air battery by allowing air to diffuse in. However, it should be noted that in this integrated system, the charging rate of ZIHSC is highly dependent on the electrochemical performance of Zn-

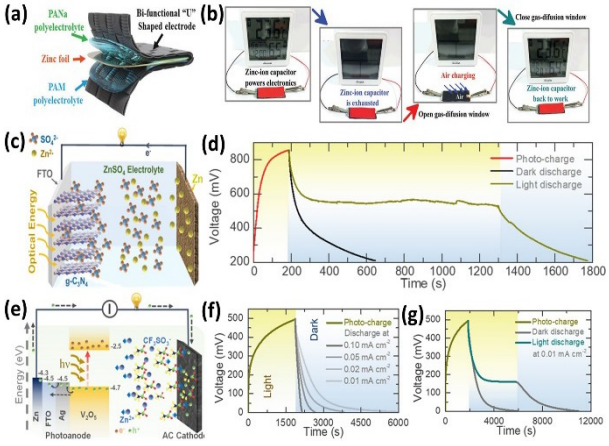

Figure 10. a) Schematic illustration of the designed air-rechargeable ZIHSC. b) The working mechanism of air-charging ZIHSC to power the hygrometer when the ZIHSC is exhausted. (a–b) Reproduced from Ref. [70] with permission. Copyright 2019, Wiley-VCH. c) Schematic illustration of the photo-rechargeable ZIHSC. d) Photo-charged (λ ~ 420 nm, intensity ~ 50 mW cm^{-2}, red) and discharged at 10 mA g^{-1} in dark (black) and illuminated (dark yellow) conditions of the assembled photo-rechargeable ZIHSC. (c-d) Reproduced from Ref. [71] with permission. Copyright 2020, American Chemical Society. e) Schematic representation of the assembled photo-rechargeable ZIHSC. f) Photo-charge (λ ~ 455 nm, intensity ~ 12 mW cm^{-2}) and discharge at different current densities (0.1 to 0.01 mA cm^{-2}) of the assembled photo-rechargeable ZIHSC. g) Photo-charge and discharge at 0.01 mA cm^{-2} in dark and illuminated conditions of the assembled photo-rechargeable ZIHSC. (e–g) Reproduced from Ref. [72] with permission. Copyright 2020, American Chemical Society.

air battery, which also suffers from Zn metal corrosion and dendrites and consequent short cycle life and irreversibility.

Regarding to the above mentioned issue, it is proposed to develop devices with energy storage and harvesting simultaneously. Regenerative and clean solar power is another source can be harvested and utilized. For example, a photo-rechargeable ZIHSC was assembled with graphitic carbon nitride as capacitor electrode and light harvesting material simultaneously (Figure 10(c)).[71] This fabricated photo-rechargeable ZIHSC could be charged and operated in a continuous light powered mode (Figure 10(d)). A photo-charged specific capacitance of ~11 F/g, an energy density of ~0.7 Wh/kg, and a power density of ~16 W/kg and capacitance retention of ~90% over 1000 cycles were obtained. However, photo-charging conversion efficiency was as low as 0.01%, which is anticipated to be enhanced by optimizing electrode composition and morphology. A similar photo-rechargeable ZIHSC was developed with vanadium oxide nanofibers as an optical and electrochemical capacitor electrode (Figure 10(e)).[72] The photo-charged capacitance and energy density was enhanced to ~138 F/g and ~4.8 Wh/kg, respectively. Extended cycling life of 4000 cycles was achieved without degradation under both dark and illumination states. A ~63% capacity increase was obtained under illumination and photo-recharge process was completed in 30 minutes (Figure 10(f)). The photo-conversion efficiency increased to ~0.05%. More efforts are required for enhanced photo-conversion efficiency.

7. Challenges and Outlook

In this review, the recent advances of ZIHSC are discussed, including explorations of cathode materials, mechanism understanding, strategies to suppress Zn dendrites and corrosion, electrolyte modifications for multi-functionalities, and assembly of integrated systems. It should be noted that the developments of ZIHSC are still at infancy stage. There are still some challenges to overcome. The main challenge is that the possible resultant intermediates, electrolyte/electrode interfaces, ion migration and solvation effect, and energy storage mechanisms during electrochemical process are still unclear and require further clarifications. Hence, various characterization techniques especially operando/in-situ analysis are desirable to conduct in ZIHSC. For example, spectroscopy characterizations, including in-situ X-ray powder diffraction (XRD), X-ray photoelectron spectroscopy (XPS), Raman spectroscopy and Fourier transform infrared spectroscopy (FTIR)), would be helpful to detect phase transformation and intermediate phase of electrode materials, and investigate chemical interactions on electrode/electrolyte interfaces and physical adsorption behaviors on electrode surfaces. Imaging techniques, such as transmission electron microscopy (TEM) and X-ray microscopy, are able to provide atomic-resolution images and record morphology evolution of electrodes. Theoretical investigations, such as electric field simulation, chemisorption energy computation and molecular dynamics emulation, can reveal homogeneity of ion distribution and diffusion, ion solvation sheath, ion diffusion pathways and the accompanied energy barriers during Zn deposition/stripping process. These techniques are beneficial to clarify the influences of electrodes/electrolytes on electrochemical performance and give insights into Zn corrosion and dendrite growth to evaluate the proposed strategies and methods. Also, the large size and strong electrostatic repulsion of Zn^{2+} might inevitably limit the charge storage kinetics and stability of host materials, thus energy storage systems incorporating other charge carriers (e.g. H^+, Li^+, Na^+) with higher diffusion kinetics are also of interest.[73] Co-intercalation of H^+ and Zn^{2+} are observed in metal oxide-based cathode materials (including MnO_2,[74] $MnO_2H_{0.16}(H_2O)_{0.27}$,[75] $Zn_{0.3}V_2O_5 \cdot 1.5H_2O$,[76] NaV_3O_8. $1.5H_2O$[77]) in ZIBs employing zinc salt based aqueous electrolyte. Addition of alkaline metal salts into zinc salts were also attempted to construct dual-ion batteries, as has been demonstrated for V_2O_5,[78] $LiMn_2O_4$,[79] Fe-hexacyanoferrate,[80] and $Li_3V_2(PO_4)_3$.[81] The hybrid charge carriers in electrolyte often enable higher capacity, high power density, and better stability. This concept is not emphasized in this review, yet it will be interesting to be incorporated into ZIHSCs.

Another challenge is the huge gap between laboratory study and practical applications. Small-sized coin-cells or pouch cells of ZIHSC are normally assembled and measured at laboratory-level conditions. By contrast, large mass loading of active materials and high charge/discharge current densities are required in practical use, which would inevitably decrease utilization rate of active materials, increase dendrite edge size, worsen dendrite growth issue and degrade lifespan and electrochemical performance of ZIHSC. Furthermore, volumetric energy/power density should be also emphasized and evaluated for large-scale practical applications. Hence, exploring thin and hydrophilic separators, adding minimum electrolytes and optimizing assembly configurations are advised to conduct in ZIHSC to minimize the total volume. Zn corrosion and hydrogen evolution at Zn anode side is another critical challenge that needs to be resolved in aqueous ZIHSCs for commercialization. These loose by-products from Zn corrosion would result in continuous consumption of electrolytes and Zn anode, leading to increased hydrogen evolution, enhanced internal pressure as well as severe dendrite formations. It indicates that Zn corrosion would result in limited shelf-life and possible explosion of sealed ZIHSCs. Improving chemical resistivity of Zn anode is of significance in ZIHSCs for practical applications. Zn surface modification is one effective strategy to mitigate/avoid Zn corrosion and the corresponding consequences.

For further developments of ZIHSCs, it is recommended to explore new cathode materials with enhanced capacities, physically and chemically modify Zn anode surface and electrolytes to suppress Zn anode corrosion and dendrite formations and thus prolong the shelf-life of ZIHSCs. Additionally, it is encouraged to introduce more functionalities into ZIHSCs, such as biodegradability, stretchability and self-healing capacity, flexibility and anti-freezing properties, for practical applications. Self-driven integrated systems, such as air-rechargeable and

photo-rechargeable ZIHSCs, are also desirable to add values to the functionalities.

For flexible/stretchable ZIHSC, mechanical deformations (twisting and bending) need to be demonstrated during charge/discharge process as well. Nevertheless, the mechanical deformations would inevitably lead to shape change with distorted regions and large curvature radii, where localized electric field are strengthened. Non-uniform ion diffusion would consequently deteriorate dendrite formation and result in short circuit/failure of ZIHSC. It becomes even worse at high current densities in practical applications. Thus, interfacial contact between gel electrolytes and Zn anode needs to be reinforced in commercialized flexible ZIHSC.

Acknowledgements

The authors acknowledge the funding support by the National Research Foundation, Prime Minister's Office, Singapore, under its Campus for Research Excellence and Technological Enterprise (CREATE) program. P.S.L. acknowledges the funding support from the National Research Foundation Investigatorship (NRF-NRFI201605).

Conflict of Interest

The authors declare no conflict of interest.

Keywords: Zn-ion hybrid supercapacitors · cathode · anode · electrolyte · multi-functionality.

[1] a) J.-Y. Hwang, S.-T. Myung, Y.-K. Sun, *Adv. Funct. Mater.* **2018**, *28*, 1802938; b) Y. Zhang, S. Liu, Y. Ji, J. Ma, H. Yu, *Adv. Mater.* **2018**, *30*, 1706310; c) J. Chen, S. Li, V. Kumar, P. S. Lee, *Adv. Energy Mater.* **2017**, *7*, 1700180; d) J. Chen, D. H. Chua, P. S. Lee, *Small Methods* **2020**, *4*, 1900648.
[2] a) A. Eftekhari, M. Mohamedi, *Mater. Today* **2017**, *6*, 211–229; b) X. Yu, S. Yun, J. S. Yeon, P. Bhattacharya, L. Wang, S. W. Lee, X. Hu, H. S. Park, *Adv. Energy Mater.* **2018**, *8*, 1702930; c) S. Wang, Q. Wang, W. Zeng, M. Wang, L. Ruan, Y. Ma, *Nano-Micro Lett.* **2019**, *11*, 70–81.
[3] a) S. Li, J. Chen, M. Cui, G. Cai, J. Wang, P. Cui, X. Gong, P. S. Lee, *Small* **2017**, *13*, 1602893; b) S. Li, J. Chen, X. Gong, J. Wang, P. S. Lee, *Small* **2018**, *14*, 1804035.
[4] L. Dong, W. Yang, W. Yang, Y. Li, W. Wu, G. Wang, *J. Mater. Chem. A* **2019**, *7*, 13810–13832.
[5] a) S. Li, J. Chen, X. Gong, J. Wang, P. S. Lee, *NPG Asia Mater.* **2018**, *10*, 406–416; b) S. Li, J. Chen, X. Gong, J. Wang, P. S. Lee, *Small* **2018**, *14*, 1804035; c) Q. Yang, Q. Li, Z. Liu, D. Wang, Y. Guo, X. Li, Y. Tang, H. Li, B. Dong, C. Zhi, *Adv. Mater.* **2020**, *32*, 2001854; d) Y. Zhang, Z. Wang, D. Li, Q. Sun, K. Lai, K. Li, Q. Yuan, X. Liu, L. Ci, *J. Mater. Chem. A* **2020**, *8*, 22874–22885.
[6] X. Ma, J. Cheng, L. Dong, W. Liu, J. Mou, L. Zhao, J. Wang, D. Ren, J. Wu, C. Xu, F. Kang, *Energy Storage Mater.* **2019**, 20, 335–342.
[7] a) Q. Chen, J. Jin, Z. Kou, C. Liao, Z. Liu, L. Zhou, J. Wang, L. Mai, *Small* **2020**, *16*, 2000091; b) H. Wang, M. Wang, Y. Tang, *Energy Storage Mater.* **2018**, *13*, 1–7.
[8] a) L. Dong, W. Yang, W. Yang, C. Wang, Y. Li, C. Xu, S. Wan, F. He, F. Kang, G. Wang, *Nano-Micro Lett.* **2019**, *11*, 94–102; b) J. Yin, W. Zhang, W. Wang, N. A. Alhebshi, N. Salah, H. N. Alshareef, *Adv. Energy Mater.* **2020**, *10*, 2001705.
[9] Z. Li, D. Chen, Y. An, C. Chen, L. Wu, Z. Chen, Y. Sun, X. Zhang, *Energy Storage Mater.* **2020**, *28*, 307–314.
[10] Y. Lu, Z. Li, Z. Bai, H. Mi, C. Ji, H. Pang, C. Yu, J. Qiu, *Nano Energy* **2019**, *66*, 104132.
[11] C. Jiang, Z. Zou, *Diamond Relat. Mater.* **2020**, *101*, 107603.
[12] a) Z. Pan, Z. Lu, L. Xu, D. Wang, *Appl. Surf. Sci.* **2020**, *510*, 145384; b) D. Wang, Z. Pan, Z. Lu, *Microporous Mesoporous Mater.* **2020**, *306*, 110445.
[13] S. Chen, L. Ma, K. Zhang, M. Kamruzzaman, C. Zhi, J. A. Zapien, *J. Mater. Chem. A* **2019**, *7*, 7784.
[14] Y. G. Lee, G. H. An, *ACS Appl. Mater. Interfaces* **2020**, *12*, 41342.
[15] Y. Zheng, W. Zhao, D. Jia, Y. Liu, L. Cui, D. Wei, R. Zheng, J. Liu, *Chem. Eng. J.* **2020**, *387*, 124161.
[16] P. Yu, Y. Zeng, Y. Zeng, H. Dong, H. Hu, Y. Liu, M. Zheng, Y. Xiao, X. Lu, Y. Liang, *Electrochim. Acta* **2019**, *327*, 134999.
[17] G.-H. An, *Appl. Surf. Sci.* **2020**, *530*, 147220.
[18] Z. Li, D. Chen, Y. An, C. Chen, L. Wu, Z. Chen, Y. Sun, X. Zhang, *Energy Storage Mater.* **2020**, *28*, 307–314.
[19] J. Yin, W. Zhang, W. Wang, N. A. Alhebshi, N. Salah, H. N. Alshareef, *Adv. Energy Mater.* **2020**, *10*, 2001705.
[20] a) D. Wang, S. Wang, Z. Lu, *Int. J. Energy Res.* **2020**; b) Y.-G. Lee, G.-H. An, *ACS Appl. Mater. Interfaces* **2020**, *12*, 41342.
[21] P. Yu, Y. Zeng, Y. Zeng, H. Dong, H. Hu, Y. Liu, M. Zheng, Y. Xiao, X. Lu, Y. Liang, *Electrochim. Acta* **2019**, *327*, 134999.
[22] Y. Li, P. Lu, P. Shang, L. Wu, X. Wang, Y. Dong, R. He, Z.-S. Wu, *J. Energy Chem.* **2021**, *56*, 404–411.
[23] Y. Tian, R. Amal, D.-W. Wang, *Front. Energy Res.* **2016**, *4*, 34–47 .
[24] G. Sun, H. Yang, G. Zhang, J. Gao, X. Jin, Y. Zhao, L. Jiang, L. Qu, *Energy Environ. Sci.* **2018**, *11*, 3367–3374.
[25] Y. Zheng, W. Zhao, D. Jia, Y. Liu, L. Cui, D. Wei, R. Zheng, J. Liu, *Chem. Eng. J.* **2020**, *387*, 124161.
[26] T. Xiong, Y. Shen, W. S. V. Lee, J. Xue, *Nano Mater. Sci.* **2020**, *2*, 159–163.
[27] L. Zhang, D. Wu, G. Wang, Y. Xu, H. Li, X. Yan, *Chin. Chem. Lett.* **2020**, *6*, 37–43.
[28] X. Zhang, Z. Pei, C. Wang, Z. Yuan, L. Wei, Y. Pan, A. Mahmood, Q. Shao, Y. Chen, *Small* **2019**, *15*, 1903817.
[29] Z. Jian, N. Yang, M. Vogel, S. Leith, A. Schulte, H. Schönherr, T. Jiao, W. Zhang, J. Müller, B. Butz, X. Jiang, *Adv. Energy Mater.* **2020**, *10*, 2002202.
[30] Z. Liu, G. Li, T. Cui, A. Borodin, C. Kuhl, F. Endres, *J. Solid State Electrochem.* **2017**, *22*, 91–101.
[31] Z. Huang, A. Chen, F. Mo, G. Liang, X. Li, Q. Yang, Y. Guo, Z. Chen, Q. Li, B. Dong, C. Zhi, *Adv. Energy Mater.* **2020**, *10*, 2001024.
[32] Q. Yang, Z. Huang, X. Li, Z. Liu, H. Li, G. Liang, D. Wang, Q. Huang, S. Zhang, S. Chen, C. Zhi, *ACS Nano* **2019**, *13*, 8275–8283.
[33] Q. Wang, S. Wang, X. Guo, L. Ruan, N. Wei, Y. Ma, J. Li, M. Wang, W. Li, W. Zeng, *Adv. Electron. Mater.* **2019**, *5*, 1900537.
[34] C. Huang, X. Zhao, Y. Xu, Y. Zhang, Y. Yang, A. Hu, Q. Tang, X. Song, C. Jiang, X. Chen, *ACS Sustainable Chem. Eng.* **2020**, *8*, 16028–16036.
[35] F.-Z. Cui, Z. Liu, D.-L. Ma, L. Liu, T. Huang, P. Zhang, D. Tan, F. Wang, G.-F. Jiang, Y. Wu, *Chem. Eng. J.* **2021**, *405*, 127038.
[36] L. Dong, X. Ma, Y. Li, L. Zhao, W. Liu, J. Cheng, C. Xu, B. Li, Q.-H. Yang, F. Kang, *Energy Storage Mater.* **2018**, *13*, 96–102.
[37] a) Q. Chen, J. Jin, Z. Kou, C. Liao, Z. Liu, L. Zhou, J. Wang, L. Mai, *Small* **2020**, *16*, 2000091; b) J. Chen, P. S. Lee, *Adv. Energy Mater.* **2021**, *11*, 2003311.
[38] a) J. Hao, X. Li, X. Zeng, D. Li, J. Mao, Z. Guo, *Energy Environ. Sci.* **2020**, *13*, 3917–3949; b) Z. Zhao, X. Fan, J. Ding, W. Hu, C. Zhong, J. Lu, *ACS Energy Lett.* **2019**, *4*, 2259–2270; c) B.-Q. Li, S.-Y. Zhang, B. Wang, Z.-J. Xia, C. Tang, Q. Zhang, *Energy Environ. Sci.* **2018**, *11*, 1723–1729; d) D. Stock, S. Dongmo, F. Walther, J. Sann, J. R. Janek, D. Schröder, *ACS Appl. Mater. Interfaces* **2018**, *10*, 8640–8648; e) K. Wippermann, J. Schultze, R. Kessel, J. Penninger, *Corros. Sci.* **1991**, *32*, 205–230.
[39] S. Siahrostami, V. Tripković, K. T. Lundgaard, K. E. Jensen, H. A. Hansen, J. S. Hummelshøj, J. S. Mýrdal, T. Vegge, J. K. Nørskov, J. Rossmeisl, *Phys. Chem. Chem. Phys.* **2013**, *15*, 6416–6421.
[40] M. Liu, X. Pu, Z. Cong, Z. Liu, T. Liu, Y. Chen, J. Fu, W. Hu, Z. L. Wang, *ACS Appl. Mater. Interfaces* **2019**, *11*, 5095–5106.
[41] a) X. Zeng, J. Hao, Z. Wang, J. Mao, Z. Guo, *Energy Storage Mater.* **2019**, *20*, 410–437; b) Q. Yang, G. Liang, Y. Guo, Z. Liu, B. Yan, D. Wang, Z. Huang, X. Li, J. Fan, C. Zhi, *Adv. Mater.* **2019**, *31*, 1903778.
[42] a) D. Han, S. Wu, S. Zhang, Y. Deng, C. Cui, L. Zhang, Y. Long, H. Li, Y. Tao, Z. Weng, *Small* **2020**, *16*, 2001736; b) W. Guo, Z. Cong, Z. Guo, C. Chang, X. Liang, Y. Liu, W. Hu, X. Pu, *Energy Storage Mater.* **2020**, *30*, 104–112; c) J. Hao, X. Li, S. Zhang, F. Yang, X. Zeng, S. Zhang, G. Bo, C. Wang, Z. Guo, *Adv. Funct. Mater.* **2020**, *30*, 2001263.
[43] Q. Zhang, J. Luan, X. Huang, L. Zhu, Y. Tang, X. Ji, H. Wang, *Small* **2020**, *16*, 2000929.

[44] X. Xie, S. Liang, J. Gao, S. Guo, J. Guo, C. Wang, G. Xu, X. Wu, G. Chen, J. Zhou, *Energy Environ. Sci.* **2020**, *13*, 503–510.
[45] Q. Zhang, J. Luan, Y. Tang, X. Ji, H. Wang, *Angew. Chem. Int. Ed.* **2020**, *59*, 13180–13191; *Angew. Chem.* **2020**, *132*, 13280–13291.
[46] a) J. Hao, B. Li, X. Li, X. Zeng, S. Zhang, F. Yang, S. Liu, D. Li, C. Wu, Z. Guo, *Adv. Mater.* **2020**, *32*, 2003021; b) C. Deng, X. Xie, J. Han, Y. Tang, J. Gao, C. Liu, X. Shi, J. Zhou, S. Liang, *Adv. Funct. Mater.* **2020**, *30*, 2000599; c) Y. Tang, C. Liu, H. Zhu, X. Xie, J. Gao, C. Deng, M. Han, S. Liang, J. Zhou, *Energy Storage Mater.* **2020**, *27*, 109–116.
[47] Z. Zhao, J. Zhao, Z. Hu, J. Li, J. Li, Y. Zhang, C. Wang, G. Cui, *Energy Environ. Sci.* **2019**, *12*, 1938–1949.
[48] Z. Cai, Y. Ou, J. Wang, R. Xiao, L. Fu, Z. Yuan, R. Zhan, Y. Sun, *Energy Storage Mater.* **2020**, *27*, 205–211.
[49] a) Z. Cao, P. Zhuang, X. Zhang, M. Ye, J. Shen, P. M. Ajayan, *Adv. Energy Mater.* **2020**, *10*, 2001599; b) M. Li, J. Meng, Q. Li, M. Huang, X. Liu, K. A. Owusu, Z. Liu, L. Mai, *Adv. Funct. Mater.* **2018**, *28*, 1802016; c) Y. Zeng, X. Zhang, R. Qin, X. Liu, P. Fang, D. Zheng, Y. Tong, X. Lu, *Adv. Mater.* **2019**, *31*, 1903675.
[50] G. H. An, J. Hong, S. Pak, Y. Cho, S. Lee, B. Hou, S. Cha, *Adv. Energy Mater.* **2020**, *10*, 1902981.
[51] X. Zhang, Z. Pei, C. Wang, Z. Yuan, L. Wei, Y. Pan, A. Mahmood, Q. Shao, Y. Chen, *Small* **2019**, *15*, 1903817.
[52] G.-H. An, S. Cha, J. I. Sohn, *Appl. Surf. Sci.* **2019**, *467*, 1157–1160.
[53] Q. Zhang, J. Luan, L. Fu, S. Wu, Y. Tang, X. Ji, H. Wang, *Angew. Chem. Int. Ed.* **2019**, *58*, 15841–15847; *Angew. Chem.* **2019**, *131*, 15988–15994.
[54] Q. Zhang, J. Luan, X. Huang, L. Zhu, Y. Tang, X. Ji, H. Wang, *Small* **2020**, *16*, 2000929.
[55] C. Li, X. Shi, S. Liang, X. Ma, M. Han, X. Wu, J. Zhou, *Chem. Eng. J.* **2020**, *379*, 122248.
[56] J. Guo, J. Ming, Y. Lei, W. Zhang, C. Xia, Y. Cui, H. N. Alshareef, *ACS Energy Lett.* **2019**, *4*, 2776–2781.
[57] a) B.-S. Lee, S. Cui, X. Xing, H. Liu, X. Yue, V. Petrova, H.-D. Lim, R. Chen, P. Liu, *ACS Appl. Mater. Interfaces* **2018**, *10*, 38928–38935; b) C. Shen, X. Li, N. Li, K. Xie, J.-g. Wang, X. Liu, B. Wei, *ACS Appl. Mater. Interfaces* **2018**, *10*, 25446–25453; c) W. Li, K. Wang, M. Zhou, H. Zhan, S. Cheng, K. Jiang, *ACS Appl. Mater. Interfaces* **2018**, *10*, 22059–22066.
[58] L. Dong, W. Yang, W. Yang, H. Tian, Y. Huang, X. Wang, C. Xu, C. Wang, F. Kang, G. Wang, *Chem. Eng. J.* **2020**, *384*, 123355.
[59] H. Yang, Z. Chang, Y. Qiao, H. Deng, X. Mu, P. He, H. Zhou, *Angew. Chem. Int. Ed.* **2020**, *59*, 9377–9381; *Angew. Chem.* **2020**, *132*, 9463–9467.
[60] Y. Huang, M. Zhong, Y. Huang, M. Zhu, Z. Pei, Z. Wang, Q. Xue, X. Xie, C. Zhi, *Nat. Commun.* **2015**, *6*, 1–8.
[61] K. Liu, A. Pei, H. R. Lee, B. Kong, N. Liu, D. Lin, Y. Liu, C. Liu, P.-C. Hsu, Z. Bao, *J. Am. Chem. Soc.* **2017**, *139*, 4815–4820.
[62] K. A. Owusu, X. Pan, R. Yu, L. Qu, Z. Liu, Z. Wang, M. Tahir, W. A. Haider, L. Zhou, L. Mai, *Mater. Today* **2020**, *18*, 100529–100536.
[63] C. Wang, Z. Pei, Q. Meng, C. Zhang, X. Sui, Z. Yuan, S. Wang, Y. Chen, *Angew. Chem. Int. Ed.* **2021**, *60*, 990–997; *Angew. Chem.* **2021**, *133*, 1003–1010.
[64] J. Hao, J. Long, B. Li, X. Li, S. Zhang, F. Yang, X. Zeng, Z. Yang, W. K. Pang, Z. Guo, *Adv. Funct. Mater.* **2019**, *29*, 1903605.
[65] W. Xu, K. Zhao, W. Huo, Y. Wang, G. Yao, X. Gu, H. Cheng, L. Mai, C. Hu, X. Wang, *Nano Energy* **2019**, *62*, 275–281.
[66] Z. Huang, A. Chen, F. Mo, G. Liang, X. Li, Q. Yang, Y. Guo, Z. Chen, Q. Li, B. Dong, *Adv. Energy Mater.* **2020**, *10*, 2001024.
[67] Q. Rong, W. Lei, L. Chen, Y. Yin, J. Zhou, M. Liu, *Angew. Chem. Int. Ed.* **2017**, *56*, 14159–14163; *Angew. Chem.* **2017**, *129*, 14347–14351.
[68] L. Han, H. Huang, X. Fu, J. Li, Z. Yang, X. Liu, L. Pan, M. Xu, *Chem. Eng. J.* **2020**, *392*, 123733.
[69] C. Huang, X. Zhao, Y. Xu, Y. Zhang, Y. Yang, A. Hu, Q. Tang, X. Song, C. Jiang, X. Chen, *ACS Sustainable Chem. Eng.* **2020**, *8*, 16028–16036.
[70] L. Ma, Y. Zhao, X. Ji, J. Zeng, Q. Yang, Y. Guo, Z. Huang, X. Li, J. Yu, C. Zhi, *Adv. Energy Mater.* **2019**, *9*, 1900509.
[71] B. D. Boruah, A. Mathieson, B. Wen, C. Jo, F. Deschler, M. De Volder, *Nano Lett.* **2020**, *20*, 5967–5974.
[72] B. D. Boruah, B. Wen, S. Nagane, X. Zhang, S. D. Stranks, A. Boies, M. De Volder, *ACS Energy Lett.* **2020**, *5*, 3132–3139.
[73] D. Chen, M. Lu, D. Cai, H. Yang, W. Han, *J. Energy Chem.* **2021**, *54*, 712–718.
[74] W. Sun, F. Wang, S. Hou, C. Yang, X. Fan, Z. Ma, T. Gao, F. Han, R. Hu, M. Zhu, C. Wang, *J. Am. Chem. Soc.* **2017**, *139*, 9775–9778.
[75] Q. Zhao, X. Chen, Z. Wang, L. Yang, R. Qin, J. Yang, Y. Song, S. Ding, M. Weng, W. Huang, J. Liu, W. Zhao, G. Qian, K. Yang, Y. Cui, H. Chen, F. Pan, *Small* **2019**, *15*, 1904545.
[76] L. Wang, K.-W. Huang, J. Chen, J. Zheng, *Sci. Adv.* **2019**, *5*, eaax4279–4289.
[77] F. Wan, L. Zhang, X. Dai, X. Wang, Z. Niu, J. Chen, *Nat. Commun.* **2018**, *9*, 1656–1666.
[78] D. Batyrbekuly, S. Cajoly, B. Laik, J. P. Pereira-Ramos, N. Emery, Z. Bakenov, R. Baddour-Hadjean, *ChemSusChem* **2020**, *13*, 724–731.
[79] R. Trocoli, A. Morata, M. Fehse, M. Stchakovsky, A. Sepulveda, A. Tarancon, *ACS Appl. Mater. Interfaces* **2017**, *9*, 32713–32719.
[80] Q. Yang, F. Mo, Z. Liu, L. Ma, X. Li, D. Fang, S. Chen, S. Zhang, C. Zhi, *Adv. Mater.* **2019**, *31*, 1901521.
[81] C. Li, W. Yuan, C. Li, H. Wang, L. Wang, Y. Liu, N. Zhang, *Chem. Commun.* **2021**.

Manuscript received: February 3, 2021
Revised manuscript received: March 14, 2021
Accepted manuscript online: March 16, 2021
Version of record online: May 4, 2021